BIOCHEMISTRY
including biophysical chemistry & molecular biology

Article

pubs.acs.org/biochemistry

Morin Inhibits the Early Stages of Amyloid β-Peptide Aggregation by Altering Tertiary and Quaternary Interactions to Produce "Off-Pathway" Structures

Justin A. Lemkul and David R. Bevan*

Department of Biochemistry, Virginia Tech, Blacksburg, Virginia 24061, United States

Supporting Information

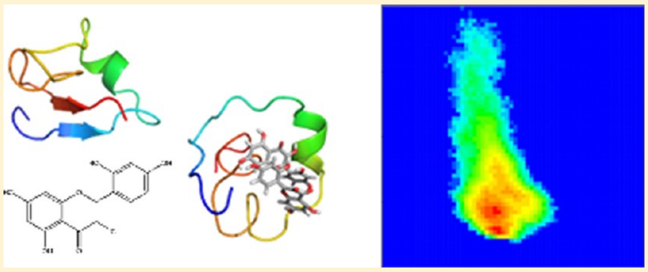

ABSTRACT: Alzheimer's disease is a debilitating neurodegenerative disorder whose pathology has been linked to the aggregation and deposition of the amyloid β-peptide (Aβ) in neural tissue. A truly effective therapeutic agent remains elusive, and attention has recently turned to the use of natural products as effective antiaggregation compounds, directly targeting Aβ. Although a wealth of in vitro and in vivo evidence suggests these compounds or their derivatives might be beneficial, a detailed understanding of the mechanism by which they act remains largely unknown. Using atomistic, explicit-solvent molecular dynamics simulations, we have investigated the association of the flavonoid morin with Aβ monomers and dimers. Through 90 simulations totaling 23.65 μs, we found that treatment of Aβ peptides with morin largely does not affect secondary structure content, unless a large molar excess of morin is present. However, in simulations of Aβ monomers and dimers, morin affected the tertiary and quaternary structure of Aβ, even at low concentrations that have been used experimentally. Thus it appears that despite the inability of morin to fully block Aβ aggregation or β-strand formation, we observe structures with altered tertiary and quaternary interactions, which may represent "off-pathway" aggregates that have been proposed previously. The simulations presented here add important new details to the mechanism of these processes.

The central dogma of the "amyloid hypothesis" holds that aggregation and deposition of the amyloid β-peptide (Aβ) in the brain are pathological phenomena in the progression of Alzheimer's disease,[1] an affliction that is the sixth-leading cause of death in the United States. While large, insoluble fibrils of Aβ were the first histological marker of the disease, it has more recently been determined that smaller, soluble oligomers of Aβ are the principal toxic species,[2] likely through interactions with cell membranes.[3] It is for this reason that Aβ has emerged as a potential drug target in the treatment of Alzheimer's disease.

Aβ is a 4-kDa peptide, produced from the amyloid precursor protein (APP) by sequential proteolysis by β- and γ-secretases.[4] Since γ-secretase cleavage is imprecise,[5] the length of Aβ is variable, with the 40- and 42-residue forms being the most common. Efforts to design inhibitors of these proteases have met with mixed success, since the activity of both enzymes is necessary for normal neuronal function.[6] In some cases, loss of γ-secretase activity has been found to exacerbate the symptoms of Alzheimer's disease.[7] Instead of targeting the enzymes that produce Aβ, recent efforts have focused on identifying compounds that directly target the aggregation of Aβ.[6,8,9] Natural compounds, such as flavonoids that are found in beverages such as tea and red wine, have emerged as viable candidates for further investigation, due to their intrinsic bioavailability and low toxicity at therapeutically relevant levels.[10]

Although numerous experimental studies have concluded that flavonoids can inhibit Aβ aggregation and destabilize Aβ fibrils,[9,11] the mechanism by which these molecules exert their effects remains somewhat unclear. In order to develop viable therapeutics for the treatment of Alzheimer's disease, molecular insight into the functionally relevant features of the putative therapeutic compound and the specific target location(s) on Aβ is necessary. In our earlier work,[12] we proposed a mechanism by which morin destabilizes Aβ protofibrils, and likely full-length fibrils, but the mechanism by which morin inhibits the formation of smaller, more toxic, oligomers is still unexplored. Such information is crucial to the development of effective anti-Aβ therapeutics.

Since experimental high-resolution structural characterization of the intermediates in the Aβ aggregation pathway remains challenging, computational methods play an important role in examining the specific interactions in the formation of toxic oligomers and higher-order Aβ assemblies. In particular, molecular dynamics (MD) simulations can provide atomic-level detail into Aβ unfolding and aggregation, as well as compounds that may inhibit this process. The utility of atomistic MD simulations to investigate these types of systems has been demonstrated previously in a number of studies.[13−18]

Received: January 25, 2012
Revised: June 25, 2012
Published: July 5, 2012

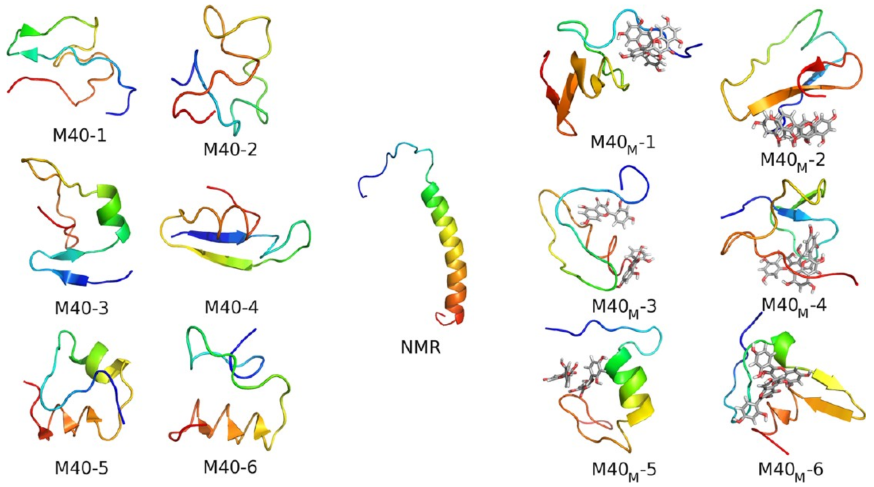

Figure 1. Aβ_{40} structures. The starting structure (1BA4, from NMR) is centered between the final snapshots of M40 (left) and M40$_M$ (right) systems. Peptides are rendered as cartoons and colored using a gradient from blue (N-terminus) to red (C-terminus). Morin molecules are shown as sticks and colored by element (C = gray, H = white, O = red).

Studies of Aβ dimerization are very limited and generally make use of coarse grain models of the peptide,[19,20] though atomistic, implicit-solvent Monte Carlo studies have also recently been conducted.[21,22] Here, we employ the first atomistic, explicit-solvent MD simulations to our knowledge that explore the binding of morin to Aβ monomers and dimers, with the goal of elucidating the mechanism by which this flavonoid inhibits the formation of toxic Aβ oligomers.

■ METHODS

System Construction. The coordinates of monomeric Aβ_{40} and Aβ_{42} were taken from PDB entries 1BA4[23] and 1IYT,[24] respectively. For fibril-derived Aβ_{40} and Aβ_{42} dimers, a pair of peptides was extracted from the coordinate files of fibril models proposed by Petkova et al.[25] and Lührs et al.,[26] respectively. An additional Aβ_{42} dimer structure was taken from the NMR structure determined by Yu et al.[27] Each of these structures was missing between 8 and 16 N-terminal residues, which were built in the xLeap module of AmberTools,[28] assigning a fully extended configuration to the amino acid backbone, similar to the approach taken by Masman et al.[29] These coordinates were aligned with the existing residues in VMD[30] to create full-length Aβ dimers. Over the course of our simulations, these residues tended to disorder (discussed below), as is expected, given that the residue positions were not assigned in the NMR structures.

For systems containing two Aβ peptides that were not yet aggregated, the final configurations of monomer simulations (described below and shown in Figures 1 and 3) were used. Peptide pairs were combined at random and positioned in an arbitrary orientation, such that the minimum distance between all atoms was at least 1.4 nm. Three systems each of Aβ_{40} and Aβ_{42} nonaggregated dimers were prepared in this manner.

All peptide systems were centered in rhombic dodecahedral boxes with a minimum solute-box distance of 1.0 nm. Parameters for all species were taken from the GROMOS96 53A6 force field.[31] For morin, parameters were taken from our previous work.[12] SPC water[32] was used as a solvent, and all systems contained ~100 mM NaCl, including counterions to compensate for the net −3 charge on each Aβ peptide. For systems containing morin, these molecules were placed randomly in the unit cell prior to solvation (see Supporting Information, Figure S1). All morin-treated systems contained a 2:1 mol ratio of morin/Aβ, except certain monomer simulations (denoted with a subscript "XM," indicating systems with excess morin) which contained a 10:1 mol ratio.

The size of our simulation systems gives rise to concentrations of Aβ and morin in the millimolar range, above the solubility of morin and beyond concentrations of Aβ that are normally used in vitro. Producing systems with absolute quantitative agreement with experiments is not possible. To do so would require systems that are orders of magnitude larger and would contain millions of atoms, precluding the collection of long simulations that produce reliable statistics. The 2:1 mol ratio of morin/Aβ is designed to model the in vitro conditions used by Ono et al. at the highest concentration of morin.[11] The 10:1 mol ratio has not been explored in vitro to our knowledge, but serves as a theoretical examination of whether or not there are any concentration-dependent effects of morin−Aβ interactions. Other investigators have used similar 10:1 mol ratios in studies of Aβ interactions with EGCG,[33] naproxen,[34] and ibuprofen.[35] We believed our approach would yield results that would be directly comparable to those studies.

Simulation Protocol. All simulations were performed using the GROMACS package, version 4.0.7.[36] All systems were energy-minimized using the steepest descent method. Equilibration was then conducted in two phases, during which position restraints were placed on all heavy protein atoms. The first phase applied an NVT ensemble for 50 ps, using the Berendsen weak coupling method[37] to maintain the temperature of the system at 310 K. The protein and solvent (including ions and morin, if applicable) were coupled separately. The second phase of equilibration applied an NPT ensemble for 50 ps, using the Nosé-Hoover thermostat[38,39] and Parrinello-Rahman barostat[40,41] to maintain temperature (310 K) and pressure (1 bar), respectively. Production MD was then conducted in the absence of any restraints, using the same NPT ensemble. Simulations of Aβ monomers were conducted for 150 ns, while all dimer systems were simulated for at least 250 ns. Simulations were stopped after the backbone root-mean-square deviation (rmsd) of the Aβ peptides was stable for at least 100 ns (as determined by block averaging), over which time data were analyzed. As a consequence, some simulations

Table 1. Simulation System Designators, Contents, and Trajectory Lengths[a]

classification	system type	contents	designator	system size (atoms)	simulation length (ns)
monomers	Aβ_{40} monomer	1BA4	M40	24,145	150 ns × 6
	Aβ_{40} monomer + morin	M40 + 2 morin	$M40_M$	24,140	150 ns × 6
		M40 + 10 morin	$M40_{XM}$	24,018	150 ns × 6
	Aβ_{42} monomer	1IYT	M42	23,546	150 ns × 6
	Aβ_{42} monomer + morin	M42 + 2 morin	$M42_M$	23,535	150 ns × 6
		M42 + 10 morin	$M42_{XM}$	23,425	150 ns × 6
dimers	Aβ_{40} dimers	M40-1 + M40-6	$D40_1$	44,693	450 ns × 1
					250 ns × 1
					400 ns × 1
		M40-2 + M40-5	$D40_2$	39,818	500 ns × 1
					550 ns × 1
					600 ns × 1
		M40-3 + M40-4	$D40_3$	48,212	250 ns × 1
					500 ns × 1
					450 ns × 1
	Aβ_{40} dimers + morin	$D40_1$ + 4 morin	$D40_{1M}$	44,584	450 ns × 1
					300 ns × 1
					250 ns × 1
		$D40_2$ + 4 morin	$D40_{2M}$	39,739	250 ns × 2
					500 ns × 1
		$D40_3$ + 4 morin	$D40_{3M}$	48,178	750 ns × 1
					450 ns × 1
					250 ns × 1
	Aβ_{42} dimers	M42-1 + M42-6	$D42_1$	51,693	450 ns × 1
					250 ns × 1
					350 ns × 1
		M42-2 + M42-5	$D42_2$	55,057	250 ns × 2
					550 ns × 1
		M42-3 + M42-4	$D42_3$	61,414	250 ns × 2
					500 ns × 1
	Aβ_{42} dimers + morin	$D42_1$ + 4 morin	$D42_{1M}$	51,632	250 ns × 2
					350 ns × 1
		$D42_2$ + 4 morin	$D42_{2M}$	55,002	250 ns × 1
					300 ns × 1
					500 ns × 1
		$D42_3$ + 4 morin	$D42_{3M}$	61,362	450 ns × 1
					400 ns × 1
					500 ns × 1
preformed dimers	Aβ_{40} fibril-derived dimer	Petkova Aβ_{40} dimer	P40	91,797	250 ns × 3
	Aβ_{40} fibril-derived dimer + morin	P40 + 4 morin	$P40_M$	91,742	250 ns × 3
	Aβ_{42} fibril-derived dimer	Lührs Aβ_{42} dimer	L42	107,583	250 ns × 3
	Aβ_{42} fibril-derived dimer + morin	L42 + 4 morin	$L42_M$	107,507	250 ns × 3
	Aβ_{42} soluble dimer	Yu Aβ_{42} dimer	Y42	84,526	250 ns × 3
	Aβ_{42} soluble dimer + morin	Y42 + 4 morin	$Y42_M$	84,474	250 ns × 3

[a] The multiplier in the final column indicates the number of replicates of a given trajectory length. Hyphenated designators indicate an individual numbered replicate within a set. For instance, "M40-1" indicates replicate 1 of the M40 set, which were simulations of Aβ_{40} monomers. Likewise, "M42" indicates simulations of Aβ_{42} monomers. "D40" and "D42" represent simulations of two Aβ peptides from the M40 and M42 sets, respectively. "P40", "L42", and "Y42" indicate simulations of different models of preformed Aβ dimers. The subscript "M" indicates the presence of morin, "XM" indicates a large molar excess of morin (explained in the main text), and any subscripted numerals indicate an individual simulation set.

were considerably longer than 250 ns. Simulation systems, their designators, and a tabulation of individual simulation times are given in Table 1. The total simulation time, for all systems and all replicates, was 23.65 μs.

All simulations employed three-dimensional periodic boundary conditions. All bond lengths were constrained using P-LINCS,[42] allowing an integration time step of 2 fs. The neighbor list was cut off at 1.4 nm and updated every 10 fs. All short-range nonbonded interactions were cut off at 1.4 nm, with dispersion correction applied to energy and pressure terms to account for the truncation of van der Waals interactions. Long-range electrostatic interactions were calculated with the smooth particle mesh Ewald method[43,44] using cubic-spline interpolation and a Fourier grid spacing of approximately 0.12 nm. All analyses were conducted using programs in the GROMACS package. Secondary structure was assigned according to the DSSP algorithm.[45] All applicable results were assessed using a two-tailed *t* test, and results classified as being statistically significant if $p < 0.05$.

Table 2. Structural Parameters for Monomeric Aβ_{40} Peptides Averaged over the Last 100 ns of Simulation Time[a]

	initial value	M40	M40$_M$	M40$_{XM}$
total helix[b] (%)	45	7 ± 8	10 ± 11	15 ± 9
β-strand[c] (%)	0	20 ± 12	17 ± 7	11 ± 6
bend (%)	10	24 ± 7	22 ± 8	16 ± 4
turn (%)	10	12 ± 8	12 ± 7	20 ± 8
random coil (%)	65	36 ± 7	39 ± 6	39 ± 8
rmsd (nm)	N/A	1.1 ± 0.1	1.03 ± 0.06	0.85 ± 0.08[d]
R_g (nm)	1.375 ± 0.005	1.00 ± 0.05	1.04 ± 0.04	1.1 ± 0.1[d]
heavy atom contacts (count)	9013 ± 73	9713 ± 221	9373 ± 317	8808 ± 783[d]
hydrophobic contacts (count)	1619 ± 26	1950 ± 38	1789 ± 66[d]	1650 ± 232[d]
intrapeptide hydrogen bonds (count)	24 ± 2	23 ± 3	21 ± 1	18 ± 5
backbone hydrogen bonds (count)	18.7 ± 0.8	12 ± 3	11 ± 3	11 ± 2

[a] All entries reflect averages with standard deviations from six simulations in each set. Initial values indicate the average of these parameters in all six equilibrated structures. [b] Total helix is the sum of α-, 3_{10}-, and π-helical content. [c] β-strand content reflects the sum of extended β-strand and isolated β-bridge structures. [d] Significantly different from control (M40) simulations, as determined by a two-tailed t test with $p < 0.05$.

RESULTS

Simulations of Aβ_{40} Monomers. During the simulations in the M40 set, much of the initial helicity of Aβ_{40} was lost in favor of random coil elements and short β-strands (Figure 1 and Table 2). In two simulations (M40-5 and M40-6, see Figure 1), short, parallel three-stranded β-sheets formed. In three of the remaining M40 simulations (M40-1, M40-3, and M40-4), antiparallel β-hairpins developed in N-terminal and central regions of Aβ_{40}. In all simulations, the peptide adopted a collapsed structure, converging to an average R_g of 1.00 ± 0.05 nm, while simultaneously increasing heavy atom contacts by 8% over the final 100 ns of the six replicate simulations (Table 2 and Figure 2A). Hydrophobic contacts increased by 20% from the equilibrated structures (Table 2 and Figure 2C). The greater relative increase in hydrophobic contacts (as compared to all heavy atom contacts) indicates that the structural changes observed in Aβ_{40} were driven by the formation of a stable hydrophobic nucleus in the structure.

Hydrogen bonding patterns also changed over the course of the M40 simulations. In the initial, equilibrated structure of Aβ_{40}, there were approximately 24 intrapeptide hydrogen bonds, of which 19 (79.2%) involved backbone groups. Over time, as Aβ_{40} collapsed and lost much of its initial helicity, 24 ± 3 total intrapeptide hydrogen bonds persisted, but only half of these involved backbone groups (Table 2). The native backbone hydrogen bonding pattern changed substantially, such that while the total number of intrapeptide hydrogen bonds was effectively constant, many of the initially interacting backbone groups became exposed to solvent as other, non-native hydrogen bonds developed.

The Aβ_{40} peptides in simulations in the presence of morin (M40$_M$) behaved similarly to those of the M40 set described above. Aβ_{40} had a tendency to become more collapsed than its initial configuration, with an average R_g comparable to that of the M40 set (Table 2). Binding of morin had only a small effect on the overall secondary structural characteristics of Aβ_{40}, decreasing β-strand content to 17 ± 7% and increasing total helicity and random coil content to 10 ± 11% and 39 ± 6%, respectively (Table 2). Morin interacted equally with backbone and side chain moieties on Aβ_{40}, forming 2.1 ± 0.9 hydrogen bonds with backbone groups and 2.3 ± 0.8 with side chain groups. These hydrogen bonds competed for intraprotein hydrogen bonds, reducing the total number of intraprotein hydrogen bonds relative to the M40 simulations (Table 2).

The most pronounced effect of morin binding to Aβ_{40} was a reduction in the number of hydrophobic contacts formed within Aβ_{40}. Fewer heavy atom contacts were formed within Aβ_{40} in the M40$_M$ simulations than in the M40 simulations (Table 2 and Figure 2B), and the final value of 9373 ± 317 represents an increase of 4% from the initial value present in the NMR structure (Table 2). Structural changes of Aβ are expected due to the difference in environment in which the structure was obtained (SDS micelles) and what was used here (water). Such metrics serve as a useful reference point for measuring structural parameters in the presence and absence of morin. In addition, hydrophobic contacts were significantly reduced compared to the M40 results (Table 2 and Figure 2D). In the M40$_M$ simulations, 1789 ± 66 hydrophobic contacts formed (an 11% increase from the starting value of 1619 ± 26), which was fewer than in the M40 systems (1950 ± 38), which increased by 20% relative to the starting structure. Some broadening of the energy minimum in the case of the M40$_M$ simulations is apparent (Figure 2), indicative of the ability of morin to induce greater structural heterogeneity in the final state of Aβ_{40} when exposed to 2:1 morin. Across the six replicate simulations in the M40$_M$ set, morin made contact with all residues of Aβ_{40}, at least transiently (Supporting Information, Figures S2 and S3), but the residues with which morin formed the greatest number of contacts were in the N-terminal sequence E$_3$FRHD$_7$, as well as residues Tyr10, Phe19, Phe20, Leu34, and Met35 (Supporting Information, Figure S3). In these systems, one molecule of morin was close to the N-terminal residues, while one was very far away from the peptide as a consequence of random placement (Supporting Information, Figure S1). The residency times of morin with the residues on Aβ_{40} (Supporting Information, Figure S2) suggest that, despite these initial positions, morin was able to interact with many of the residues in the peptide sequence, showing a preference for Tyr10, Phe19, Phe20, Leu34, and Met35 (Supporting Information, Figure S3).

Having examined systems that modeled experimental conditions,[9,11] we sought to explore the effects of a large molar excess of morin on the structure of Aβ_{40} in a simulation set called M40$_{XM}$, which contained a 10:1 morin/Aβ mole ratio. Though this mole ratio would only be relevant when Aβ levels are extremely low, it was of interest to determine if there was any concentration dependence on the effects observed in the M40$_M$ set. Such a mole ratio was also recently used in a simulation study by Liu et al. in the context of EGCG binding

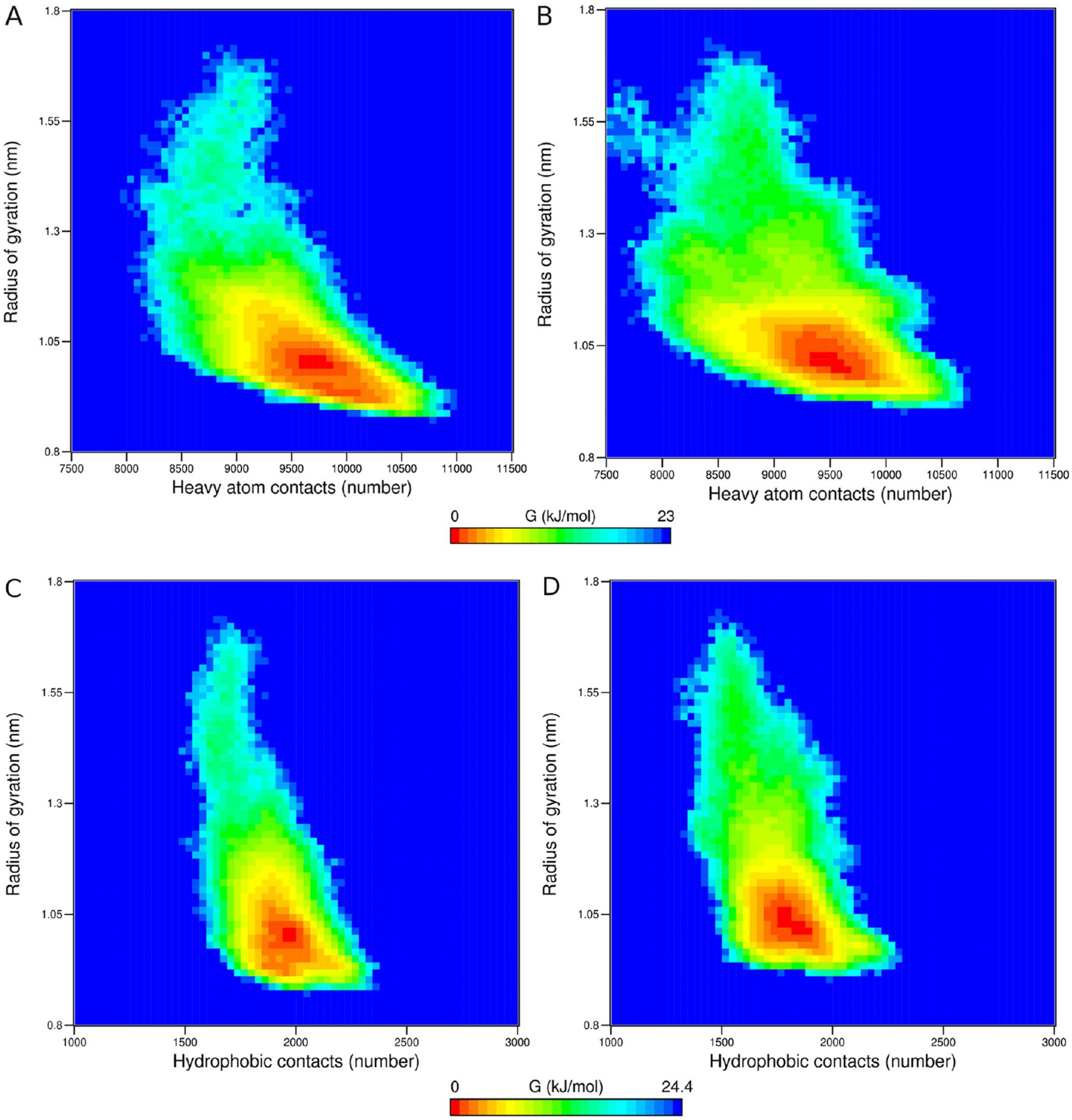

Figure 2. Gibbs free energy surfaces of R_g vs heavy atom contacts for (A) M40 and (B) M40$_M$ and R_g vs hydrophobic contacts for (C) M40 and (D) M40$_M$ simulations. Data are a composite of all six replicate simulations in each set. A contact was defined as occurring within 0.6 nm. Note that there is a slight difference in the Gibbs free energy scale between the upper and lower panels.

to Aβ.[33] In the M40$_{XM}$ set, we found that, as with the M40$_M$ set, the presence of even 10:1 morin had no significant effect on the secondary structure of Aβ_{40} (Table 2); however, like the simulations in the M40$_M$ set, both heavy atom and hydrophobic contacts were significantly reduced relative to the M40 results (Table 2), with hydrophobic contacts increasing by just 2% from the number of hydrophobic contacts initially present in the M40$_{XM}$ starting structure.

As a consequence of the fact that the high level of morin reduced the ability of Aβ_{40} to form intrapeptide contacts, the peptide remained significantly more elongated than in the M40 set, with an R_g value of 1.1 ± 0.1 nm (Table 2). In the M40$_{XM}$ systems, morin formed networks through hydrogen bonding and aromatic stacking, aligning with hydrophobic regions on the peptide and forming hydrogen bonds with Aβ_{40}. Snapshots of the final structures of each of the M40$_{XM}$ systems are shown in Figure 3.

From our analysis of monomeric Aβ_{40}, it is clear that even a large molar excess of morin, beyond the concentrations yet explored in vitro, is unable to significantly alter the secondary

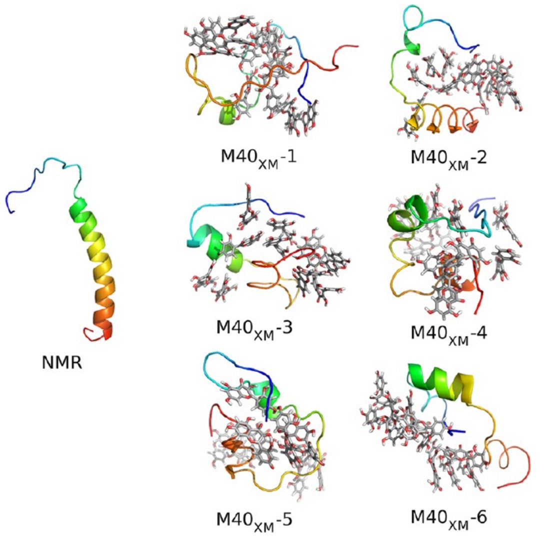

Figure 3. Aβ_{40} structures. The starting structure (1BA4, from NMR) is shown at left, alongside the final snapshots (150 ns) of the M40$_{XM}$ (right) systems. Peptides are rendered as cartoons and colored using a gradient from blue (N-terminus) to red (C-terminus). Morin molecules are shown as sticks and colored by element (C = gray, H = white, O = red).

structure content of the peptide, though the effects on tertiary structure in the M40$_{XM}$ set were augmented relative to the M40$_{M}$ simulations, indicating a concentration-dependent effect induced by the crowding and clustering of morin when associated with Aβ. At both 2:1 and 10:1 morin/Aβ, morin inhibited the formation of intrapeptide contacts, particularly hydrophobic contacts, thus interfering with the formation of a stable hydrophobic nucleus that may be critical for further aggregation. This effect can be attributed to the binding of morin to hydrophobic residues Phe19, Phe20, Leu34, and Met35 (Supporting Information, Figure S3). Thus, in the context of monomeric Aβ_{40}, it appears that morin affects tertiary, but not secondary, structure.

Simulations of Aβ_{42} Monomers. In the M42 simulations, as in the M40 simulation set described above, Aβ_{42} tended to lose its considerable initial helicity over time and adopt a more compact structure (Table 3 and Figure 4), which was an expected outcome as a result of the fact that the initial Aβ_{42} structure was determined in an organic solvent (hexafluoroisopropanol). Random coil elements were the predominant secondary structural feature (Table 3), with short β-strand structures persisting in five of the six simulations (all except M42-5, see Figure 4). Helicity was generally retained in residues within the sequence Y$_{10}$EVHHQKLVFF$_{20}$. Aβ_{42} stabilized at an average R_g of 1.00 ± 0.03 nm (Table 3), equivalent to that of Aβ_{40}. As was the case with Aβ_{40}, the Aβ_{42} peptide also established more intrapeptide heavy atom contacts over time, increasing by 4% over the final 100 ns of each of the six replicate simulations (Table 3 and Figure 5A). Hydrophobic contacts increased by 12% over these trajectories (Table 3 and Figure 5C).

As with the M40 results, the greater relative increase in hydrophobic contacts suggests a prominent role for these contacts in driving the structural conversion of Aβ_{42}. The Aβ_{42} peptides in the M42 set established a similar number of hydrophobic contacts as did the Aβ_{40} peptides in the M40 set, though the starting value for these contacts was higher in Aβ_{42} due to the kinked starting structure leading to more initial contacts in the C-terminal region. The greater number of total heavy atom contacts in M42 relative to M40 is a consequence of Aβ_{42} having two additional amino acids. Despite these subtle differences, the overall structures and level of contact within the untreated Aβ_{40} and Aβ_{42} peptides were very similar.

At the outset of the M42 simulations, there were approximately 26 total intraprotein hydrogen bonds, of which nearly all (96%) involved backbone groups (Table 3). The extensive backbone hydrogen bonding can be attributed to the considerable α-helical content present in the NMR structure, which is a result of structural determination in a nonpolar solvent.[24] As a result, over the course of our M42 simulations in water, much of the initial backbone hydrogen bonding was lost. Though 23 ± 1 total hydrogen bonds persisted in the Aβ_{42} structure over the six replicate simulations, only 47.8% involved backbone groups (Table 3), a result that is similar to the behavior of the Aβ_{40} peptides in the M40 simulation set discussed above.

The simulations of Aβ_{42} in the presence of 2:1 morin (the M42$_{M}$ series) manifested behavior similar to the M40$_{M}$ results. The Aβ_{42} peptide again tended to collapse and lose some of its initial α-helicity (Table 3), but its overall secondary structural features were essentially indistinguishable from those of untreated Aβ_{42} peptides in the M42 simulation set. Thus, as in the case of the M40$_{M}$ simulations, the presence of morin had

Table 3. Structural Parameters for Monomeric Aβ_{42} Peptides[a]

	initial value	M42	M42$_{M}$	M42$_{XM}$
total helix[b] (%)	69	15 ± 4	15 ± 5	24 ± 7[d]
β-strand[c] (%)	0	13 ± 5	11 ± 5	4 ± 5[d]
bend (%)	0	26 ± 6	26 ± 3	20 ± 6
turn (%)	23.8	8 ± 2	9 ± 4	11 ± 7
random coil (%)	7.1	38 ± 6	39 ± 3	41 ± 6
rmsd (nm)	N/A	1.2 ± 0.1	1.2 ± 0.2	1.0 ± 0.1[d]
R_g (nm)	1.504 ± 0.005	1.00 ± 0.03	1.03 ± 0.06	1.20 ± 0.07[d]
heavy atom contacts (count)	9665 ± 73	10029 ± 118	9979 ± 249	9116 ± 404[d]
hydrophobic contacts (count)	1749 ± 25	1955 ± 93	1896 ± 75	1702 ± 112[d]
intrapeptide hydrogen bonds (count)	26 ± 1	23 ± 1	23 ± 2	19 ± 3[d]
backbone hydrogen bonds (count)	25 ± 1	11 ± 1	10.6 ± 0.8	11 ± 2

[a] All entries reflect averages with standard deviations from six simulations in each set. Initial values indicate the average of these parameters in all six equilibrated structures. [b] Total helix is the sum of α-, 3_{10}-, and π-helical content. [c] β-strand content reflects the sum of extended β-strand and isolated β-bridge structures. [d] Significantly different from control (M42) simulations, as determined by a two-tailed t test with $p < 0.05$.

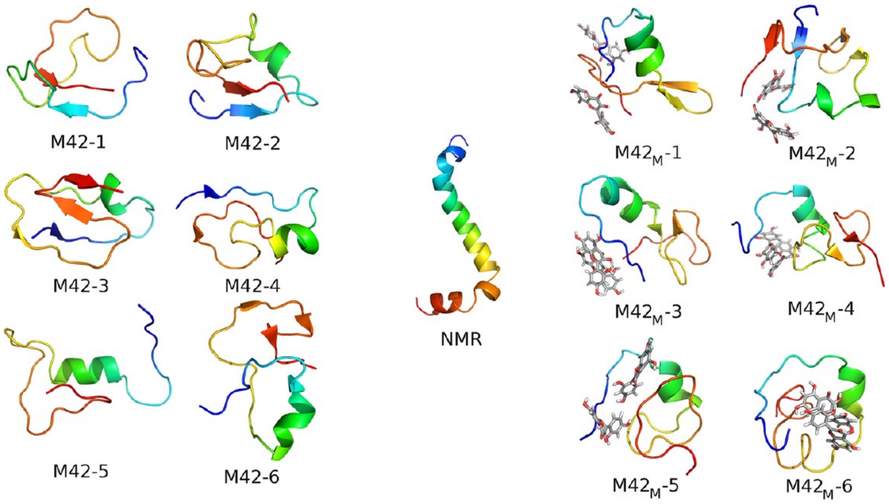

Figure 4. Aβ_{42} structures. The starting structure (1IYT, from NMR) is centered between the final snapshots of M42 (left) and M42$_M$ (right) systems. Peptides are rendered as cartoons and colored using a gradient from blue (N-terminus) to red (C-terminus). Morin molecules are shown as sticks and colored by element (C = gray, H = white, O = red).

no effect on the loss of helicity or emergence of β-strand structures. In M42$_M$ simulations, the Aβ_{42} peptide became more compact than its initial configuration; concomitant with this compaction was an increase in total and hydrophobic contacts (Table 3). Initially, there were 9678 ± 89 total heavy atom contacts within the Aβ_{42} peptide, a figure that increased by 3% over the course of the simulations. Hydrophobic contacts increased by 9%, a slightly smaller relative increase than was observed in the M42 simulations (12%). Thus, we conclude that the formation of hydrophobic contacts within the Aβ_{42} peptide was not influenced as strongly by the presence of morin as was the case for the Aβ_{40} peptide, though a measurable difference was still observed. The reason for this phenomenon can be explained by examining the residues of Aβ_{42} with which morin interacted. While morin made contact with all of the residues of Aβ_{42} in the six M42$_M$ simulations (Supporting Information, Figure S4), the contacts that were most persistent involved the same N-terminal sequence as in the M40$_M$ simulations (E$_3$FRHD$_7$), as well as Tyr10 and Phe20. Interactions between morin and the C-terminal hydrophobic residues were less pronounced than these interactions (Supporting Information, Figure S5).

It is also important to note the appearance of two minima in the free energy surfaces plotted in Figure 5B,D (total and hydrophobic contacts in Aβ_{42}, respectively). In the absence of morin (Figure 5A,C), there is a single energy minimum in both free energy surfaces. The presence of dual energy minima in the M42$_M$ simulations indicates that the presence of morin produced two clusters of configurations with comparable energy, derived from alterations to the tertiary structure of Aβ_{42} based on the location of morin binding. In trajectories where morin interacted principally with charged and polar residues in the N-terminal region of Aβ_{42} (M42$_M$-2, M42$_M$-5, and M42$_M$-6), close intrapeptide contacts were formed between the central hydrophobic cluster (CHC) of Aβ_{42} (L$_{17}$VFFA$_{21}$) and the C-terminal region, leading to more compact structures (Figure 4) that populated the free energy minimum corresponding to the smaller value of R_g (Figure 5). These N-terminal interactions are among the most frequently observed contacts in the M42$_M$ simulation set (Supporting Information, Figure S5) and thus strongly influence the structure of Aβ_{42}. In cases where morin bound to the CHC (principally Phe20) and other hydrophobic residues (M42$_M$-3 and M42$_M$-4), these contacts were reduced and Aβ_{42} was more elongated (Figure 4), leading to the free energy minimum at a greater value of R_g (Figure 5). In simulation M42$_M$-1, morin interacted with both polar and nonpolar regions on Aβ_{42}, leading to configurations that sampled both energy minima.

In the final set of simulations of Aβ monomers (the M42$_{XM}$ set), the Aβ_{42} peptide was treated with a 10:1 mol ratio of morin. This treatment produced peptide configurations that were the most native-like out of all of the M42 simulations conducted here, having the lowest backbone rmsd (Table 3). The peptide retained significantly more helical content (Table 3) and produced significantly less β-strand content than in the control M42 simulations. The Aβ_{42} peptide remained more elongated than in the M42 set, with an average R_g of 1.20 ± 0.07 nm. Both heavy atom and hydrophobic contacts were significantly reduced in the M42$_{XM}$ set compared to M42 (Table 3). These effects can be attributed to the network of morin molecules that acted to cover the peptide, shielding it from the polar solvent while simultaneously restricting its ability to collapse and interconvert its secondary structure between helical and β-strand elements. Snapshots from the end of the six replicate simulations in the M42$_{XM}$ set are shown in Figure 6.

Effect of Morin on Aβ_{40} Dimerization. To explore the process by which Aβ_{40} forms dimers in solution and the potential for morin to inhibit this process, we assembled three starting configurations of random dimer pairs, using the final configurations of the M40 simulation set as shown in Table 1. For each of the three resulting starting configurations, three independent simulations were initiated using different random velocities. This procedure resulted in nine independent trajectories in the D40 simulation set. Though there are effectively an infinite number of combinations of starting configurations and orientations that can be used to start these simulations, we feel we have established a reasonable subset here, recognizing that comprehensive sampling of all possible Aβ dimerization events would be a much larger, and perhaps intractable, task. For this reason, we analyze the data from the D40 simulation set as an aggregate, rather than considering the

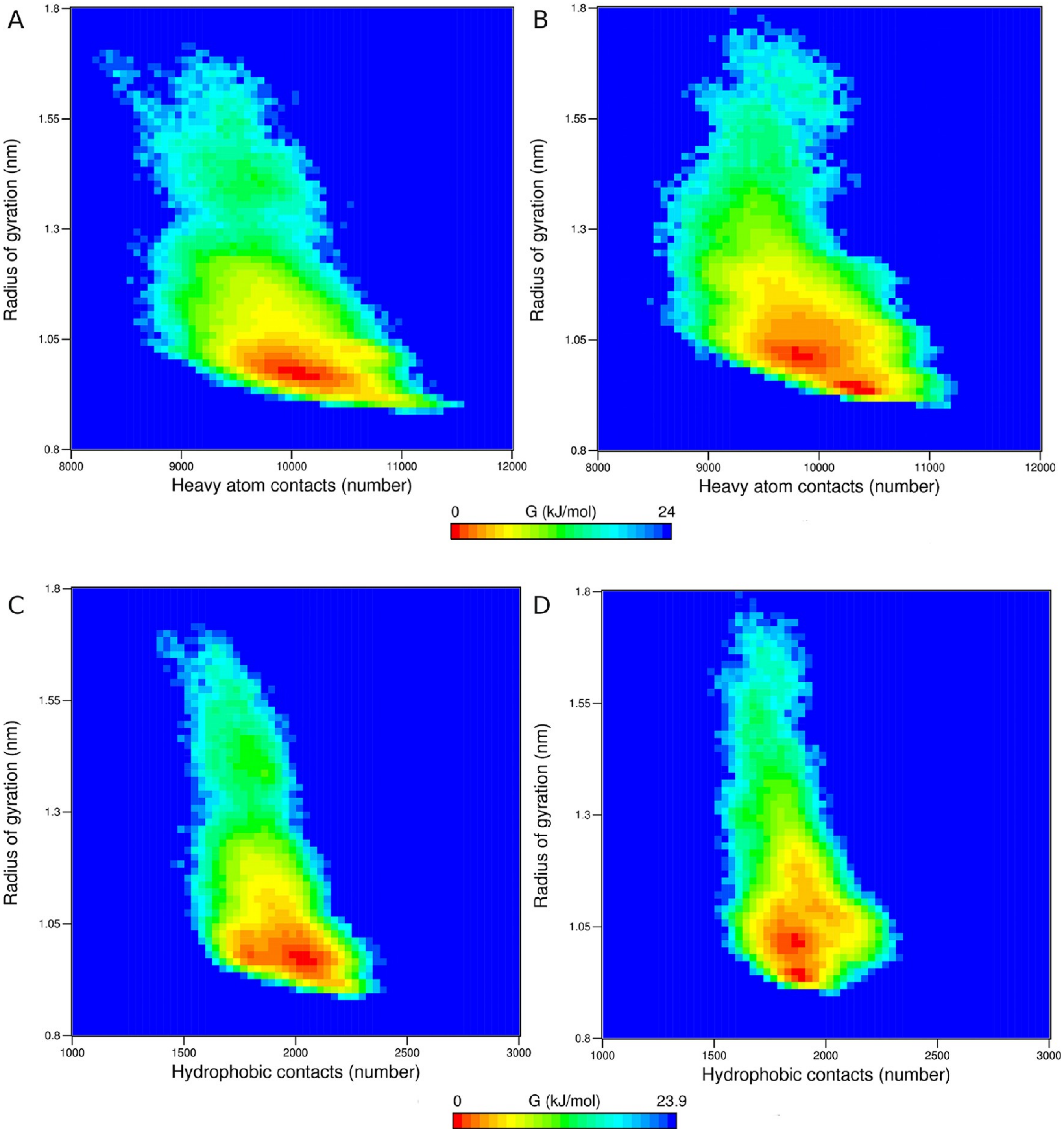

Figure 5. Gibbs free energy surfaces of R_g vs heavy atom contacts for (A) M42 and (B) $M42_M$ and R_g vs hydrophobic contacts for (C) M42 and (D) $M42_M$ simulations. Data are a composite of all six replicate simulations in each set. A contact was defined as occurring within 0.6 nm. Note that there is a slight difference in the Gibbs free energy scale between the upper and lower panels.

individual simulation subsets ($D40_1$, $D40_2$, and $D40_3$) as being distinct. All of their starting orientations are plausible and part of an infinitely large set of possible configurations, with no single subset being any more likely than the others. Representative examples will be highlighted throughout the discussion, as necessary, for particular simulations that are especially illustrative of specific phenomena.

In all D40 simulations, the $A\beta_{40}$ peptides (initially separated, with all interpeptide atomic distances greater than 1.4 nm) aggregated to form dimers. The average β-strand content over the final 100 ns of all simulations was 24 ± 5%. Total helical content was 4 ± 4% over this same time period. These values represent a slight increase in β-strand content relative to the monomeric form of $A\beta_{40}$, concomitant with a small reduction in total helical content (Table 2).

The dimerization of $A\beta_{40}$ caused the total protein solvent-accessible surface area (SASA) to decrease by 2.78% (to an average area of 72.5 ± 2.5 nm^2), with hydrophobic SASA

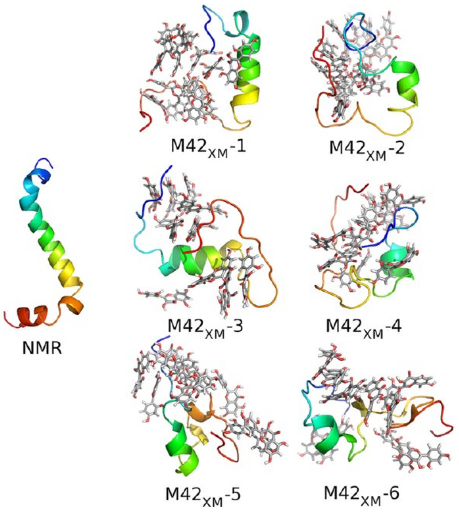

Figure 6. Aβ_{42} structures. The starting structure (1IYT, from NMR) is shown at left, alongside the final snapshots (150 ns) of the M42$_{XM}$ (right) systems. Peptides are rendered as cartoons and colored using a gradient from blue (N-terminus) to red (C-terminus). Morin molecules are shown as sticks and colored by element (C = gray, H = white, O = red).

decreasing by 2.5% and polar SASA by 2.86%. Thus, the dimerization of Aβ_{40} was driven almost equally by burial of polar and nonpolar surfaces.

The aggregation of the Aβ_{40} peptides observed in the D40 simulations produced compact structures with an average R_g of 1.25 ± 0.05 nm (Figure 7). The peptides formed 928 ± 288 heavy atom contacts, of which 244 ± 83 were hydrophobic (26.3%). In addition, 5 ± 3 interpeptide hydrogen bonds formed, with 2 ± 2 (40%) involving backbone groups. Contacts formed between all regions of the Aβ_{40} peptides, but the most common occurrence was the establishment of contacts in the central hydrophobic cluster (CHC) of the peptide, which encompasses the sequence L$_{17}$VFFA$_{21}$, and is a region known to be critical for aggregation.[46] Close interpeptide contacts were established in this region in 7 of the 9 simulations in the D40 set. Short β-hairpin structures appeared in 5 of the 9 simulations in the D40 set (D40$_1$-1, D40$_1$-2, D40$_1$-3, D40$_2$-1, and D40$_3$-1), as shown in Figure 7.

The presence of morin in the D40$_M$ simulation set did not prevent the aggregation of the Aβ_{40} peptides but did affect interpeptide interactions. Two principal binding modes emerged for morin, influencing the nature of the interpeptide interactions in different ways. The first we call "interfacial binding," in which at least two molecules of morin were present between the two Aβ peptides (i.e., at the dimerization interface). The second binding mode was termed "surface binding," which describes the cases in which the majority of the morin molecules were either clustered or scattered over the solvent-exposed surface of the Aβ peptides. In the D40$_M$ simulation set, four trajectories (D40$_{1M}$-1, D40$_{1M}$-2, D40$_{2M}$-3, and D40$_{3M}$-3) manifested interfacial binding, while the remaining five trajectories (D40$_{1M}$-3, D40$_{2M}$-1, D40$_{2M}$-2, D40$_{3M}$-1, and D40$_{3M}$-2) showed surface binding (Figure 8).

Interfacial binding of morin in the D40$_M$ set significantly ($p < 0.05$) reduced the total interpeptide heavy atom contacts (548 ± 118) and hydrophobic contacts (146 ± 40) relative to controls. That is, morin impaired the ability of the Aβ_{40} dimers to form stable hydrophobic nuclei that would normally be shielded from solvent. Interfacial binding similarly reduced the number of interpeptide backbone and total hydrogen bonds

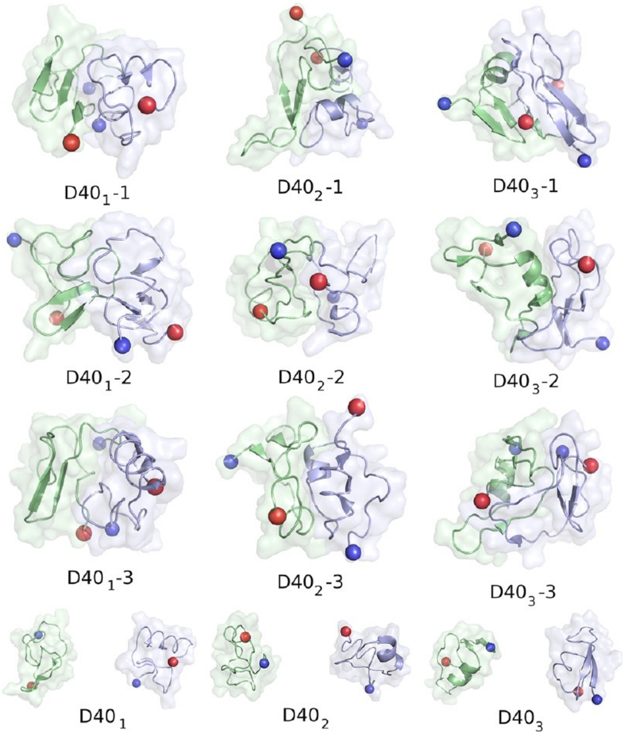

Figure 7. Structures of D40 dimers. Starting structures are shown below the final snapshots of D40 simulations. Individual peptides are rendered as cartoons and colored blue and green with an overlaid transparent surface to give an impression of overall topology. N- and C-termini are shown for each peptide as blue and red spheres, respectively.

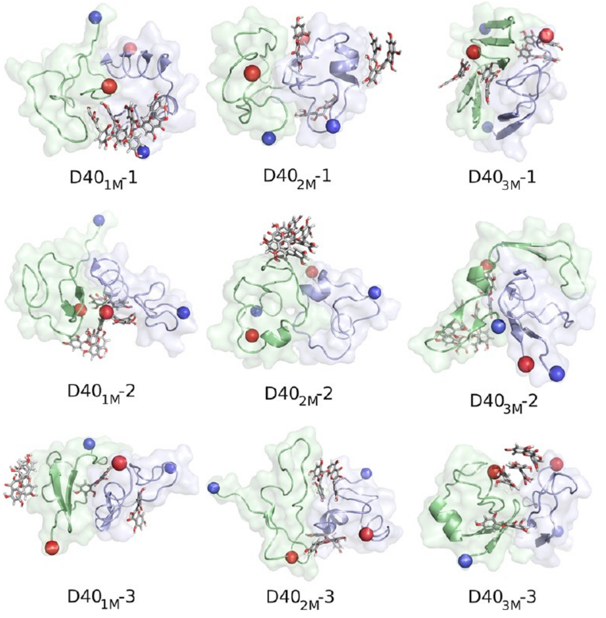

Figure 8. Structures of D40$_M$ dimers, taken from the final snapshots of D40$_M$ simulations. Peptides are rendered as in Figure 7. Morin molecules are shown as sticks and colored by element (C = gray, H = white, O = red). Starting configurations are identical to those shown in Figure 7, but with morin molecules randomly distributed in the simulation cell.

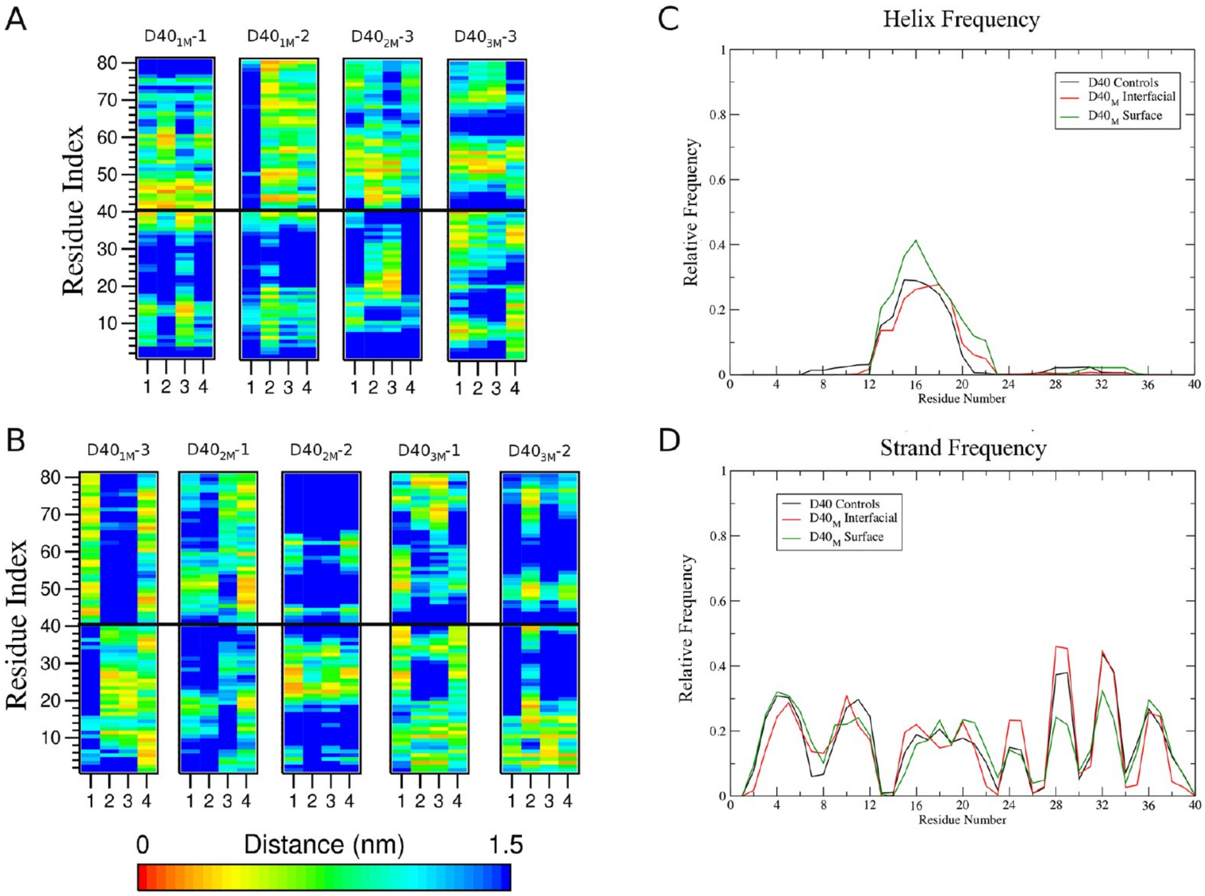

Figure 9. Distance matrices, averaged over the last 100 ns of each trajectory for D40$_M$ simulations in which morin bound (A) interfacially and (B) to the surface of the Aβ_{40} dimers. For panels (A) and (B), the residue numbering on the *y*-axis corresponds to peptides 1 (1−40) and 2 (41−80). Secondary structure frequencies for (C) total helix and (D) β-strand content, also averaged over the last 100 ns of each trajectory. Frequencies were calculated from frames pooled over all simulations in the relevant sets.

that formed over the trajectories to 1 ± 1 (a reduction of 50%) and 3 ± 1 (a reduction of 40%), respectively. The weakened interactions between the Aβ_{40} peptides in these simulations resulted in dimers with larger values of R_g (1.33 ± 0.07 nm) than those of the control D40 simulations.

Interfacial binding of morin resulted in the manifestation of less SASA (69.5 ± 2.4 nm^2), a decrease of 7.6% relative to the initial configurations; hydrophobic SASA decreased by 7.4%, and polar SASA by 8.0%. Thus, with morin present between the two peptides, a greater amount peptide surface area was buried than in controls, but as in the case of the D40 controls, there was equal burial of hydrophobic and polar surface area. It is clear from the data presented above regarding interpeptide contacts that the presence of interfacial morin inhibited the formation of a stable hydrophobic nucleus within the dimers that formed, and thus, while the manner in which Aβ_{40} aggregated was unaffected by the presence of morin (both polar and nonpolar interactions were formed) the resulting dimers interacted more weakly than in the case of the D40 controls.

Binding of morin to the dimerization interface resulted in contacts between morin and many residues in the N-terminal polar and C-terminal hydrophobic regions (Supporting Information, Figure S6), with the largest number contacts forming with Tyr10, His13, His14, Phe20, Val39, and Val40 (Supporting Information, Figure S7). Thus interfacial binding caused morin to form persistent contacts with a large number of Aβ_{40} residues, both polar and nonpolar, though interactions with the polar region including $S_{26}NK_{28}$ were very infrequent (Supporting Information, Figures S6 and S7).

In the D40 simulations, dimerization of Aβ_{40} led to an increase in β-strand content relative to the M40 monomer simulations. This behavior was observed in the case of the D40$_M$ simulations, as well, but to a lesser extent in the simulations that produced interfacial binding than in the D40 simulations. The total β-strand content in these four simulations (D40$_{1M}$-1, D40$_{1M}$-2, D40$_{2M}$-3, and D40$_{3M}$-3) was 22 ± 7%. It thus appears that despite the weakened interactions between the Aβ_{40} peptides, the overall ability of Aβ_{40} to form β-strand structures was not inhibited significantly, though some subtle changes were notable. The nature of secondary structural changes depended upon the residues with which morin interacted in these simulations (Figure 9). Interfacial binding of morin to the Aβ_{40} dimers resulted in morin making close contact with a large number of residues throughout the Aβ sequence (Figure 9A and Supporting Information, Figure S7), whereas in the case of surface binding (Figure 9B), contacts were established with more discrete regions of the peptides, particularly the N-terminal region and the polar sequence $S_{26}NK_{28}$ (Supporting Information, Figure S9). Surface binding of morin in the vicinity of residues 13−23 slightly increased the appearance of helical structures (Figure 9C) and slightly decreased the formation of β-strand structures toward the C-terminus (Figure 9D). Interfacial binding had no clear implications for secondary structure propensity of any region of the peptide.

Surface binding of morin to Aβ_{40} in the D40$_M$ simulations led to an insignificant decrease in the number of interpeptide heavy atom contacts and hydrophobic contacts (699 ± 192 and 208 ± 59, respectively). Interpeptide backbone hydrogen bonding was also reduced by 50% relative to controls (1 ± 2 per time frame), but total interpeptide hydrogen bonding was unaffected (6 ± 3 per time frame). Overall, the size of the Aβ_{40} dimers in the simulations that produced surface binding was comparable to controls, with an average R_g value of 1.27 ± 0.04 nm, indicating that these dimers were more compact than in the cases where morin bound interfacially. In the case of surface binding, morin formed a large number of contacts with only a very few residues in Aβ_{40}, namely, Arg5, Tyr10, and the $S_{26}NK_{28}$ sequence. Though transient contacts were formed with most of the residues in Aβ_{40} (Supporting Information, Figure S8), the number of contacts that persisted over the final 100 ns of each trajectory was very low except for these specific residues.

As in the cases wherein morin bound interfacially, surface binding of morin to the Aβ_{40} dimers led to a decrease in SASA relative to controls, with a total area of 68.3 ± 1.6 nm^2 observed over the final 100 ns of these simulations, a decrease of 8.6% from the SASA present in the initial configurations. Hydrophobic SASA decreased by 7.7% and polar SASA by 10.0%, both larger decreases than in the case of interfacial binding. Thus, as compared to interfacial binding of morin, surface binding resulted in slightly less surface area being exposed to solvent, which is primarily a consequence of the morin molecules coating the polar surface of the Aβ_{40} dimers, a behavior manifested in the greater relative reduction in polar SASA.

Taken together with the interpeptide contact data, it can be concluded that surface binding of morin does not significantly affect the ability of Aβ_{40} to dimerize, nor does it significantly affect the structural nature of the dimers. Surface binding of morin also had a minimal effect on the ability of Aβ_{40} to form β-strand structures, with a total content of 25 ± 16% in these simulations, a result that was indistinguishable from controls in the D40 set. Conversely, interfacial binding of morin had a more pronounced impact on the dimer structures, resulting in significantly fewer interpeptide contacts than in the D40 controls and a larger value of R_g, indicating that the interpeptide interactions in these species were weakened by the presence of morin.

Effect of Morin on Aβ_{42} Dimerization. Simulations from the D42 series were prepared in the same manner similar as those of the D40 set, deriving monomeric starting configurations from the final snapshots of the M42 simulations (Table 1). As with the D40 set, nine independent trajectories were generated (three each from three distinct starting configurations; see Figure 10). As was the case in the D40 simulations, all of the D42 simulations produced dimers of Aβ_{42} (Figure 10). Upon dimerization, the total β-strand content of Aβ_{42} nearly doubled from 13 ± 5% (in the monomeric state, see Table 3) to 25 ± 8%. The dimers observed over the course of these simulations had an average R_g of 1.30 ± 0.06 nm and formed an extensive network of intermolecular contacts. On average, 1040 ± 304 contacts were present between the Aβ_{42} peptides, of which 245 ± 62 (23.6%) were hydrophobic. Along with the formation of these contacts, an average of 9 ± 4 total interpeptide hydrogen bonds were formed, of which 4 ± 2 involved backbone groups.

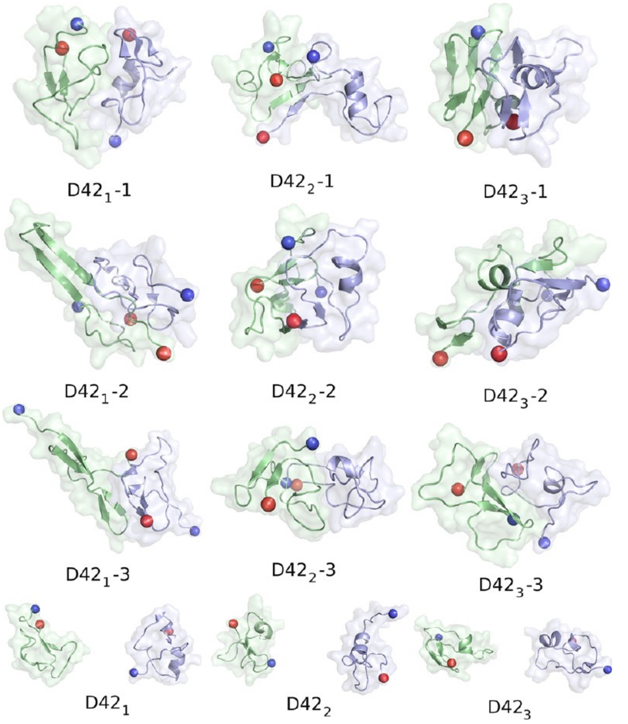

Figure 10. Structures of D42 dimers. Starting structures are shown below the final snapshots of D42 simulations. Individual peptides are rendered as cartoons and colored blue and green with an overlaid transparent surface to give an impression of overall topology. N- and C-termini are shown for each peptide as blue and red spheres, respectively.

Dimerization of Aβ_{42} in the D42 simulations led to an overall decrease in SASA, converging from a starting value of 80.7 ± 3.3 nm^2 to 75.1 ± 2.0 nm^2 over the final 100 ns of the simulations, a decrease of 6.94%. In contrast to the dimerization of Aβ_{40} in the D40 simulations, wherein both polar and nonpolar surfaces were buried equally, the formation of Aβ_{42} dimers was driven by burial of hydrophobic SASA, which decreased by 8.65%, while polar SASA decreased by 4.37%.

Whereas dimerization of Aβ_{40} in the D40 simulation set most frequently involved interactions within the CHC of the peptide, Aβ_{42} dimers formed in the D42 set were principally driven by contacts within the C-terminal regions of the peptide sequence. The CHC is flanked by a sequence to its N-terminus that is largely polar, while residues C-terminal of the CHC are mostly nonpolar. This observation explains why Aβ_{42} dimerization was mainly due to interactions between hydrophobic surfaces while Aβ_{40} dimerization was due to both polar and hydrophobic interactions.

In several of the simulations in the D42 set, elongated β-hairpin configurations resembling those found in the mature fibril state were observed (Figure 10, specifically simulations D42$_1$-2, D42$_1$-3, and D42$_3$-3). In only one simulation in the D42$_M$ (morin-treated) set was a similar conformation observed (D42$_{3M}$-3, Figure 11). The appearance of these structures in one-third of the D42 simulations is an expected behavior of Aβ_{42}, which is prone to more rapid aggregation in solution than is Aβ_{40}.[47,48] Coupled with the considerable increase in β-strand content relative to the monomeric state, it is clear that

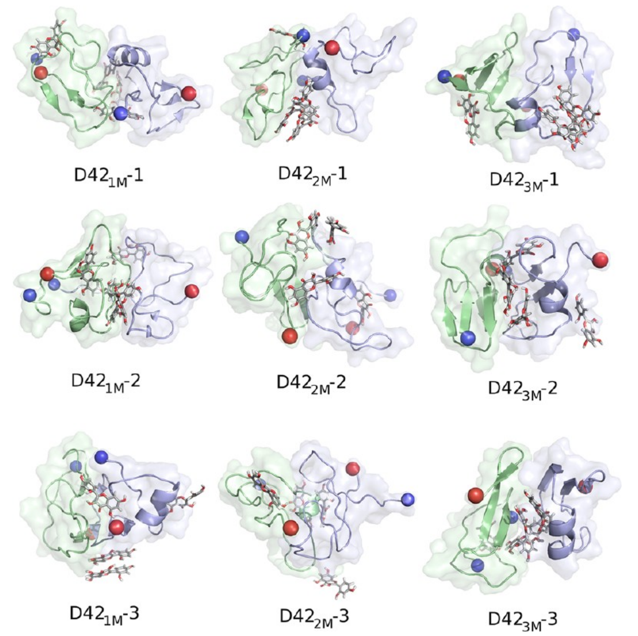

Figure 11. Structures of $D42_M$ dimers, taken from the final snapshots of $D42_M$ simulations. Peptides are rendered as in Figure 10. Morin molecules are shown as sticks and colored by element (C = gray, H = white, O = red). Starting configurations are identical to those shown in Figure 10, but with morin molecules randomly distributed in the simulation cell.

dimerization of Aβ_{42} promotes the formation of oligomeric species rich in β-strands that further propagate aggregation.

As in the $D40_M$ simulations, two binding modes for morin (interfacial and surface) were observed in the $D42_M$ simulation set (Figure 11). In the instances wherein multiple morin molecules bound at the interface of the two Aβ_{42} peptides (simulations $D42_{1M}$-2, $D42_{2M}$-1, $D42_{3M}$-2, and $D42_{3M}$-3), heavy atom contacts between the peptides were reduced to 694 ± 222, of which 170 ± 70 (24.5%) were hydrophobic. Both of these values are reduced relative to the control D42 simulations by 33.3% for heavy atom contacts and 30.6% for hydrophobic contacts. Interfacial clusters of morin principally formed in the vicinity of hydrophobic residues in the Aβ_{42} peptides, and as such they directly competed for peptide−peptide interactions in the hydrophobic, solvent-inaccessible region of the Aβ_{42} dimer. The main site of interaction between morin and Aβ_{42} in the case of interfacial binding was the CHC, particularly Phe19 and Phe20 (Supporting Information, Figures S10 and S11). Other sites in the Aβ_{42} sequence that showed a large number of contacts with morin were Phe4, Leu34, Met35, and Val36. Binding of morin in the hydrophobic core of the Aβ_{42} dimer (interfacial binding) led to an overall decrease in total SASA from an initial value of 80.6 ± 2.5 nm^2 to 70.6 ± 2.1 nm^2, a reduction of 12.3%, leaving a total SASA that was 5.9% smaller than controls in the D42 simulation set.

Interpeptide hydrogen bonding was also inhibited in the presence of interfacially bound morin, with 1.4 ± 0.7 backbone hydrogen bonds maintained over the last 100 ns of each trajectory (a significant reduction relative to D42 controls). In total, 6 ± 2 interpeptide hydrogen bonds were maintained, a 33.3% reduction relative to D42 controls. The weakening of interpeptide interactions resulted in Aβ_{42} dimers with a slightly expanded R_g, 1.33 ± 0.05 nm. There was no measurable difference in β-strand content in Aβ_{42} when morin bound interfacially within the dimers (25 ± 8% in the D42 simulations, and 24 ± 8% in these simulations).

When morin bound to the surface of Aβ_{42} dimers (simulations $D42_{1M}$-1, $D42_{1M}$-3, $D42_{2M}$-2, $D42_{2M}$-3, and $D42_{3M}$-1), heavy atom and hydrophobic contacts were reduced (816 ± 240 and 224 ± 59, respectively), although these reductions relative to controls were less dramatic than in the case of interfacially bound morin. Interpeptide hydrogen bonding was reduced, but not significantly, in these simulations (6 ± 3 total hydrogen bonds, of which 2 ± 2 involved backbone groups). In these simulations, the Aβ_{42} dimers that formed were essentially as compact as those of the control D42 simulations, with an average R_g of 1.31 ± 0.05 nm. Interestingly, the binding of morin to the surface of Aβ_{42} dimers did induce a significant reduction in β-strand content (17 ± 5%) relative to control D42 simulations (24 ± 8%), a slight increase relative to the results of the M42 monomer simulations (13 ± 5%). We attribute this behavior to the locations along the Aβ_{42} peptide to which morin bound. As in the case of the $D40_M$ simulations, the specific binding sites of morin along the Aβ sequence determined the frequency with which certain secondary structural features emerged in the $D42_M$ simulations. Interfacial binding of morin often occurred at residues in the CHC or hydrophobic C-terminus (Figure 12A), causing an increase in total helical content (Figure 12C) and decrease in β-strand probability (Figure 12D) in the CHC and residues preceding it ($H_{14}Q_{15}K_{16}$), while also increasing the appearance of helical elements between residues 24−28 (Figure 12C). Surface binding of morin had a similar effect, but the decrease in β-strand frequency in the CHC was even more pronounced (Figure 12D). When morin bound to the surface of the Aβ_{42} peptides, it principally associated with residues flanking the CHC (like Tyr10, His13, Glu22, Asp23, and Lys28 as shown in Supporting Information, Figure S13) in addition to Phe19 and Phe20 within the CHC (Figure 12B and Supporting Information, Figure S13), inhibiting the elongation of this region into a β-strand structure.

Binding of morin to the surface of $D42_M$ dimers reduced the overall SASA by 8.83%, from an initial value of 80.0 ± 3.3 nm^2 to 73.0 ± 2.3 nm^2. The subsequent reductions in hydrophobic and polar SASA were 10.4% and 6.3%. The reduction in these components of the SASA were both less than in the case of interfacial binding, indicating that even when morin bound to the surface of the Aβ_{42} dimers, the N-terminal polar regions remained solvent-exposed, causing them to be disordered rather than organized in β-strands or otherwise buried such that they form close interpeptide interactions.

We conclude from these observations that the binding of morin to hydrophobic regions of Aβ_{42} (interfacial binding) substantially alters the quaternary, but not secondary, structure of Aβ_{42} dimers. In contrast, surface binding to principally polar residues in Aβ_{42} strongly affects secondary structure, but effects on quaternary structure are diminished and the extent of peptide−peptide interactions (and thus aggregation) is comparable to control simulations. Thus, the manner in which morin binds to the Aβ_{42} peptide is critical for determining the manner in which the structure of these dimers is affected. These findings are in contrast with the results for the dimerization of the Aβ_{40} peptide, wherein the secondary structure content was largely unaffected by either interfacial or surface binding of morin. We attribute this phenomenon to the fact that Aβ_{40} dimerization buried a greater amount of polar surface area than did the Aβ_{42} peptide, which was driven

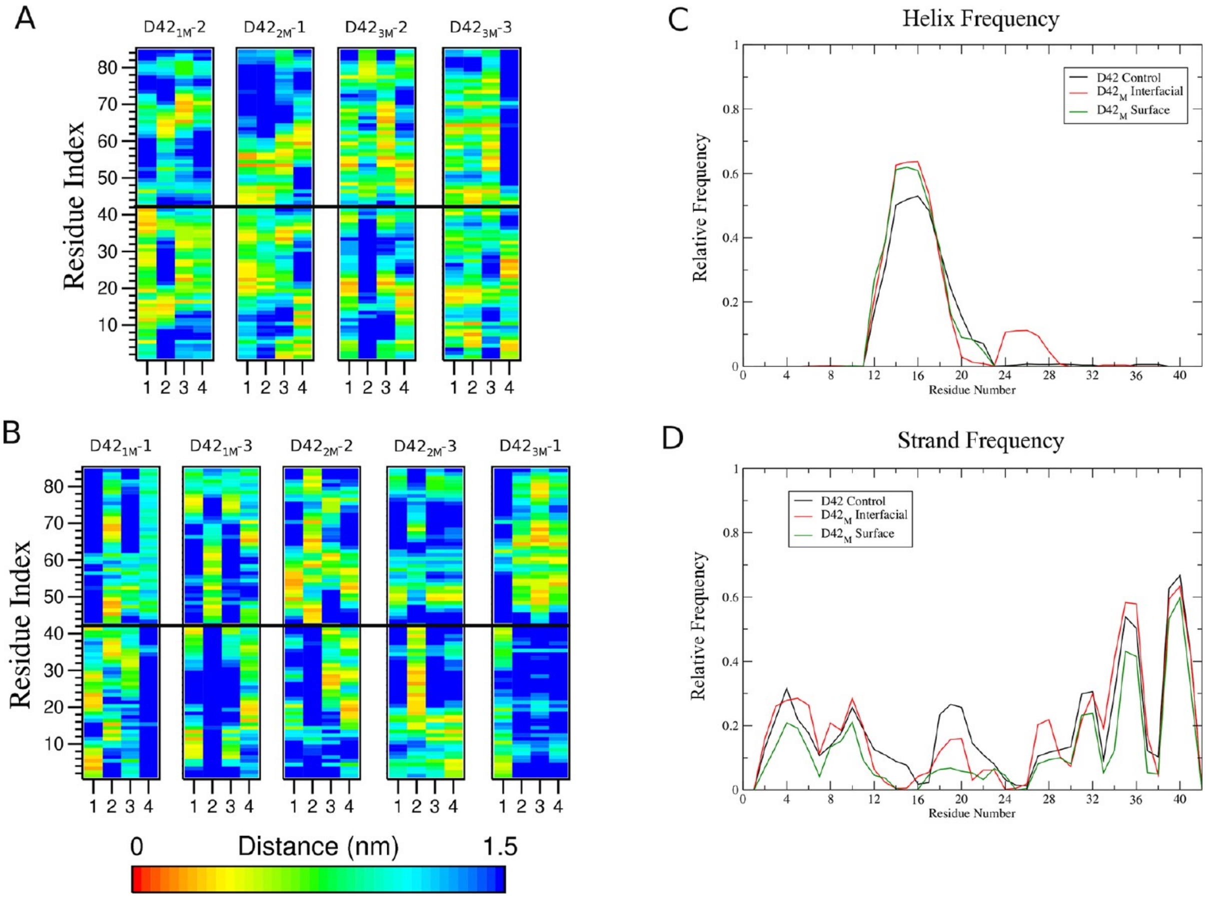

Figure 12. Distance matrices, averaged over the last 100 ns of each trajectory for D42$_M$ simulations in which morin bound (A) interfacially and (B) to the surface of the Aβ_{42} dimers. For panels (A) and (B), the residue numbering on the y-axis corresponds to peptides 1 (1−42) and 2 (43−84). Secondary structure frequencies for (C) total helix and (D) β-strand content, also averaged over the last 100 ns of each trajectory. Frequencies were calculated from frames pooled over all simulations in the relevant sets.

together by hydrophobic interactions, leaving more polar area exposed. Burial of polar surface area in the case of Aβ_{40} prevented the disruption of β-strand formation, while exposure to solvent in the case of the Aβ_{42} dimers caused the β-strand content to decrease when these residues were exposed to morin and the aqueous solvent. The fundamental differences in aggregation of these two peptides explain how morin may affect each differently.

Binding of Morin to Fibril-Derived Aβ_{40} and Aβ_{42} Dimers. In the case of preformed Aβ dimers, the effect of morin on the structural stability of these aggregates appears to be dependent upon the nature of the aggregate itself. Two models of fibril-derived dimers are considered here, one derived from the structure of the Aβ_{40} fibril,[25] and the other from the Aβ_{42} fibril.[26] There are subtle differences between these two structures in terms of intra- and interpeptide packing and orientation,[49] indicating that Aβ_{40} and Aβ_{42} may follow slightly different aggregation pathways to reach the mature fibril state. Since Aβ_{42} is generally regarded as being more toxic than Aβ_{40} due to its more rapid aggregation in solution,[47,48] understanding subtle differences in the structures of Aβ_{40} and Aβ_{42} at each stage of the aggregation cascade may be important in understanding how Aβ aggregates and how this process can be inhibited. Examining fibril-derived dimers allows us to investigate the stability of "fibril-competent" configurations, or end-stage aggregation.

In the context of the Aβ_{40} fibril-derived dimer from Petkova et al.,[25] herein referred to as P40, the control (untreated) systems showed that these dimers were very stable throughout the simulations, with a backbone rmsd of 0.80 ± 0.01 nm. The P40 dimers remained largely elongated, with an average R_g of 1.99 ± 0.02 nm. The two peptides twisted around one another during these simulations (Figure 13), a behavior that has been theorized to contribute to the stability of amyloid aggregates.[29,50,51] This twisting established an extensive network of interpeptide heavy atom contacts (2974 ± 117), an increase of 11.5% from the starting value of 2667 ± 24.

The effect of morin binding to the P40 dimers was dependent upon the region of Aβ to which morin bound. In simulation P40$_M$-1 (Figure 13), morin bound to the polar N-terminal residues of the Aβ_{40} peptides, resulting in no significant effect on the dimer structure, in terms of backbone rmsd (0.74 ± 0.08 nm), R_g (2.19 ± 0.05 nm), or interpeptide contacts (2949 ± 242). In this simulation, two morin molecules bound to the P40 dimer in monomeric form, diffusing along much of the structure before forming strong interactions with the polar N-terminal region. The other two morin molecules bound to the P40 structure as a dimer, ultimately interacting with the other monomeric morin molecules to form a tetramer (Figure 13) that persisted for the remainder of the simulation. This cluster of morin interacted principally with residues Phe4, Arg5, His6, Asp7, and Tyr10 of the Aβ sequence, forming

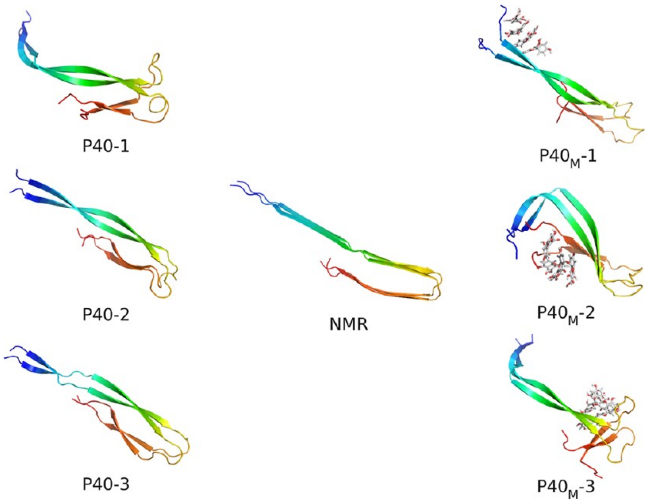

Figure 13. Petkova Aβ_{40} dimers. The starting structure (from NMR, with the missing N-terminal 8 residues reconstructed) is centered between the final snapshots of P40 (left) and P40$_M$ (right) systems. Peptides are rendered as cartoons and colored using a gradient from blue (N-terminus) to red (C-terminus). Morin molecules are shown as sticks and colored by element (C = gray, H = white, O = red).

hydrogen bonds to the polar residues and π-stacking interactions with Phe4 and Tyr10.

In simulations P40$_M$-2 and P40$_M$-3, morin bound to hydrophobic residues toward the C-terminus of the P40 dimers, destabilizing the dimer structure, manifesting in increased rmsd (1.45 ± 0.03 nm), a more collapsed structure (R_g = 1.8 ± 0.2 nm), and a slight decrease in interpeptide contacts (2920 ± 170). In simulation P40$_M$-2, one morin molecule bound to the hydrophobic C-terminal residues, while a trimeric assembly of morin molecules formed near the polar bend region. Interactions of this trimer with polar residues in the bend (most notably, Glu22, Asp23, and Ser25) led to the formation of a twisted, four-stranded β-sheet with the morin trimer spanning the CHC and bend regions. The remaining morin molecule remained tightly associated with the hydrophobic C-terminal residues, causing local perturbation of the backbone in this region. A tetrameric cluster of morin formed over time, interacting with residues in the CHC and C-terminal region (Figure 13). In P40$_M$-3, all four morin molecules aggregated in solution prior to binding to the P40 dimer structure. The morin tetramer bound to the polar bend region, and after a short time, split into two dimers, one of which dissociated from the P40 structure while the other moved to interact with residues Phe19 and Phe20 of the CHC. The morin tetramer re-formed over time, interacting with this Phe dyad and the Asp23-Lys28 salt bridge, causing the interpeptide backbone hydrogen bonds of the bend region to separate (Figure 13).

It thus appears that the most pronounced effects on the P40 dimer structure appeared when morin bound to hydrophobic residues in the Aβ sequence, particularly the CHC and C-terminal region. Upon binding to these residues, the P40 dimer adopted a more distorted conformation, a twisted β-sheet in the case of P40$_M$-2, and a perturbed dimer with disrupted backbone hydrogen bonding in the case of P40$_M$-3. Binding to polar residues toward the N-terminus of the structure (as in P40$_M$-1) did not affect the stability of the P40 dimer.

Simulations of the preformed dimer derived from the Aβ_{42} fibril, determined by Lührs et al. using NMR,[26] and herein referred to as the L42 model, showed that this dimer structure was very stable, even when treated with 2:1 morin. In the control L42 simulations, the dimer structure remained elongated (R_g = 2.0 ± 0.2 nm) over the course of the simulations, while simultaneously twisting (Figure 14) and reaching an rmsd value of 1.2 ± 0.3 nm. Because of these structural changes, the number of interpeptide heavy atom contacts stabilized at a value of 2505 ± 268, an increase of 26.4% from the starting value of 1982 ± 32. In the L42 simulations, the bend region encompassing the Asp23-Lys28 salt bridges was more flexible than in the P40 dimer simulations, resulting in configurations with propeller-like twists (Figure 14).

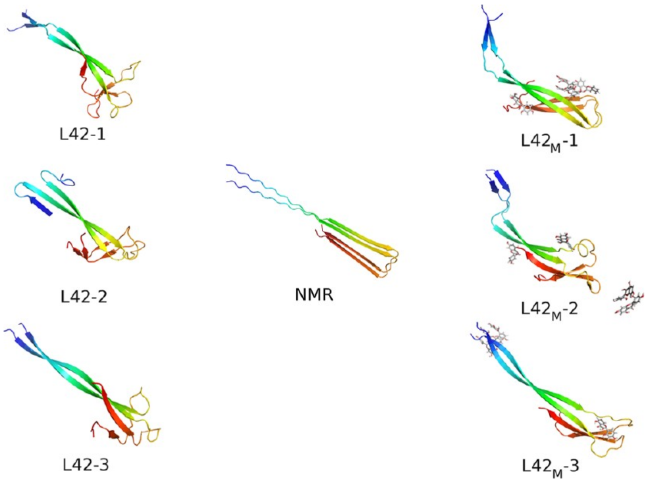

Figure 14. Lührs Aβ_{42} dimers. The starting structure (from NMR, with the missing N-terminal 16 residues reconstructed) is centered between the final snapshots of L42 (left) and L42$_M$ (right) systems. Peptides are rendered as cartoons and colored using a gradient from blue (N-terminus) to red (C-terminus). Morin molecules are shown as sticks and colored by element (C = gray, H = white, O = red).

The association of morin with the L42 dimer showed little effect in any of the three replicate L42$_M$ simulations. The Aβ_{42} dimer remained elongated (R_g = 2.1 ± 0.1 nm) and showed similar structural features to the controls. The average rmsd for Aβ_{42} dimers in the L42$_M$ set was 1.0 ± 0.2 nm, and the dimers formed 2581 ± 110 interpeptide contacts. Transient destabilization of several regions in the L42 structure was observed in these simulations and will be examined here.

In the L42$_M$-1 simulation, two morin molecules bound as monomers to the Aβ dimer, one toward the N-terminus and the other at the C-terminus. Shortly thereafter, the remaining morin molecules bound as a dimer to the bend region, destabilizing the Asp23-Lys28 salt bridge and backbone hydrogen bonding. The morin dimer then moved toward the C-terminal hydrophobic region, forming a trimer with the morin molecule already there. The backbone of the bend region re-formed some native hydrogen bonding, but the salt bridges did not re-form. For the remainder of the trajectory, the morin molecules exchanged dimer and trimer partners and resulted in the structure shown in Figure 14.

In simulation L42$_M$-2, one morin molecule bound to the N-terminal polar region, while the remaining three molecules bound as a trimer to Lys28 and Ile32. In this position, the Asp23-Lys28 salt bridge was disrupted, after which the trimer diffused toward the CHC, a phenomenon that led to distortion of the bend region. Eventually, a tetrameric morin cluster formed, covering the CHC, but this complex was short-lived, and ultimately only a dimer of morin remained bound to the L42 structure, as the remaining two molecules diffused away from Aβ after interacting with Asn27.

In the final trajectory, L42$_M$-3, two morin molecules bound as a dimer to the N-terminal polar region, while the remaining two molecules bound as monomers to the N- and C-terminal regions. Ultimately, a trimer of morin formed around Phe4, Arg5, and Asp7, while the remaining morin monomer interacted with the Asp23-Lys28 salt bridge to disrupt it and destabilize surrounding backbone hydrogen bonding.

Binding of Morin to an Oligomer-Derived Aβ_{42} Dimer. Simulations in the Y42 set modeled a dimer of Aβ_{42} that was derived from a soluble oligomer of Aβ_{42}.[27] Thus, we believe this structural model to be the most representative of the early aggregated state of Aβ_{42} both in vitro and in vivo. The structure is characterized by a pair of twisted, antiparallel intramolecular β-strands from residues 18−32 (connected by a hairpin bend from residues 23−28) and parallel intermolecular β-strands from residues 33−42 that form the dimerization interface between the two peptides. These features were well preserved during the simulations in the Y42 set (Figure 15). Over the course of these trajectories, N-terminal residues formed short β-strand structures but were principally disordered, in agreement with experimental findings.[27]

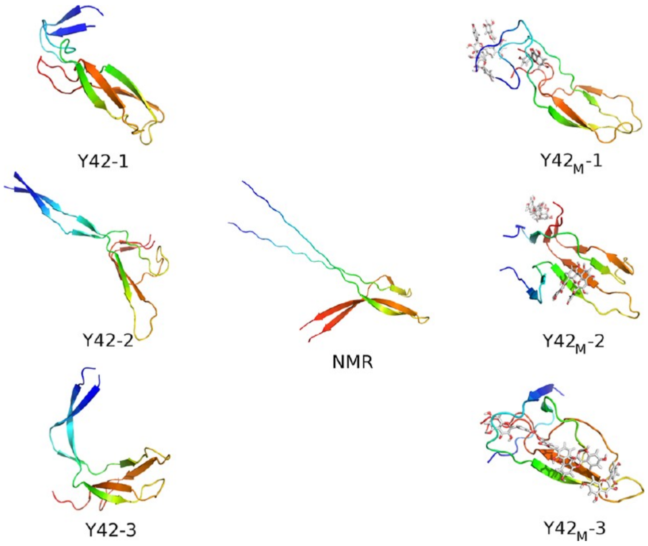

Figure 15. Yu Aβ_{42} dimers. The starting structure (from NMR, with the missing N-terminal 15 residues reconstructed) is centered between the final snapshots of Y42 (left) and Y42$_M$ (right) systems. Peptides are rendered as cartoons and colored using a gradient from blue (N-terminus) to red (C-terminus). Morin molecules are shown as sticks and colored by element (C = gray, H = white, O = red).

Though there was considerable structural heterogeneity within the dimer structures in the Y42 series, many gross structural features were consistently observed among these trajectories. The principal secondary structural elements in the Y42 dimers were β-strand (51 ± 2%) and random coil (34 ± 1%), with the remaining structure described by a combination of turns and bends. Helical content was negligible in all cases. The Y42 dimers remained largely elongated, establishing an average R_g of 1.8 ± 0.2 nm, from an initial value of 2.4 nm. This measured size is in excellent agreement with results obtained by Walsh et al.[52] Twisting and compaction of the N-terminal region of each Aβ_{42} peptide in the dimer accounted for the majority of the change in R_g (Figure 15). These structural changes amounted to an average backbone rmsd for the dimer of 1.19 ± 0.08 nm.

As the Y42 dimers twisted, the Aβ_{42} peptides increased both heavy atom contacts and interpeptide hydrogen bonding. Initially, there were 943 ± 40 heavy atom contacts between the peptides, but over the final half of the 250-ns trajectories, 2201 ± 187 contacts were established, an increase of 133.4%. In addition, there were initially just seven interpeptide hydrogen bonds within the Y42 dimers (principally in the C-terminal parallel β-strands), but over time, 22 ± 2 total interpeptide hydrogen bonds were established, of which 16 ± 4 involved backbone groups.

The addition of morin in the Y42$_M$ systems had a pronounced impact on the structure of the Aβ_{42} dimers. Binding of morin to the dimer structure (Figure 15) reduced the β-strand content of the Aβ_{42} peptides to 46 ± 4% and increased the random coil content 36 ± 5% relative to the control Y42 simulations. The Y42$_M$ dimers also became more compact than the Y42 dimers, with an average R_g of 1.5 ± 0.1 nm. Morin binding also reduced the strength of the interaction between the two peptides, such that only 1917 ± 293 heavy atom contacts and 17 ± 3 total hydrogen bonds (12.2 ± 0.8 of which involved backbone amides) persisted throughout the Y42$_M$ trajectories.

When morin associated with the Y42$_M$ dimers, the twisting present in the Y42 simulations was inhibited. Instead, β-strand structures were converted to random coils (as in Y42$_M$-3 and, to a lesser degree, Y42$_M$-1) or flattened β-sheets (Y42$_M$-2). N-terminal residues contained almost exclusively random coil structures, in contrast to Y42 simulations, in which short β-strands evolved over time. The more dramatic changes in structure induced by the binding of morin to the Aβ_{42} peptides resulted in a backbone rmsd of 1.5 ± 0.2 nm, considerably higher than the rmsd values of the Y42 dimers, 1.19 ± 0.08 nm.

In simulation Y42$_M$-1, a single morin molecule bound to polar residues including Ser8, Tyr10, and His13 and diffused along the N-terminal polar region before associating with the C-terminus and hydrophobic residues in this region. The remaining morin molecules deposited on the Y42 dimer as a trimer, which broke and re-formed over the course of the simulation, interacting with many of the polar N-terminal residues.

For the first 75 ns of Y42$_M$-2, monomeric morin molecules weakly associated with the Y42 dimer, binding and dissociating from residues in both the N-terminal and bend regions. A dimer of morin bound to Asp1 and Glu3 at approximately 98 ns, where it remained for the duration of the trajectory. The other two morin molecules bound as monomers to the bend region and nearby CHC, eventually forming a dimer that bridged these regions on both peptides, leading to the overall flattening of the Y42 dimer structure.

In the final simulation in this set, Y42$_M$-3, a morin dimer bound quickly to the Asp23-Lys28 salt bridge and was further stabilized in this location through interactions with Glu22. An additional morin molecule bound to Asn27 and diffused to associate with this dimer, forming a trimer very quickly. The final morin molecule bound to residues Phe4, Ser8, and Glu11. Over time, the morin trimer moved to associate with the CHC, and as the Y42 dimer twisted in response to these interactions, a morin tetramer formed as interactions were established among all four morin molecules (Figure 15).

■ DISCUSSION

The early stages of Aβ aggregation are crucial to the progression of Alzheimer's disease, as low molecular weight oligomeric species are highly toxic to cells.[2,3] Thus, therapeutic intervention in Alzheimer's disease is likely to be most effective during the first stages of oligomer formation. These early events in the aggregation cascade are poorly understood. Existing literature suggests that flavonoids and related compounds impede Aβ aggregation,[9] providing the motivation for the present study.

It should be noted that MD force fields have inherent limitations and biases that must be considered when interpreting the results they produce. It is important to discuss these concepts here in light of the conclusions drawn, particularly those related to secondary structure. Matthes and de Groot recently concluded that the balance between helical and extended conformations in proteins is particularly problematic.[53] These findings are one reason we consider total helical content, rather than individual α-, π-, or 3_{10}-helical structures, as they may be artifacts of the force field and not representative of a true physical state. Other force fields, however, may excessively stabilize helical structures.[54]

In light of this information, it is important to assess our results in the context of existing simulations of Aβ that have used different force fields. A number of studies have been carried out on full-length Aβ_{40} and Aβ_{42}. We use these as the basis for our comparison. Work by Flöck et al.[13] and Luttmann and Fels[14] utilized earlier versions of the GROMOS force field[55,56] and produced qualitatively similar results in terms of overall peptide structure and the evolution of its secondary structure elements. All-atom force fields such as OPLS-AA,[57] AMBER99,[58] and AMBER ff99SB[59] have been used by many other investigators and also produce similar results.[16,60−63] The results of Lee and Ham[16] for Aβ_{42} showed lower α-helical and β-strand content in favor of larger amounts of turn and coil structures than we observed, but the values of R_g were comparable to our results. Simulations using the OPEP coarse grain model[64] performed by Côté et al.[65] also produced similar structures for Aβ compared with what we observed here. Thus it appears that numerous force fields can be applied to the study of Aβ with very similar results. Olubiyi and Strodel recently demonstrated that the GROMOS96 53A6 force field (employed in the present work as well) does an excellent job of reproducing experimental NMR shifts of Aβ.[66] The secondary structure results they obtained are similar to our results, indicating that our approach of using multiple, shorter simulations produces results that agree well with the use of single, longer simulations in the microsecond range.

In our control simulations of untreated Aβ monomers, both Aβ_{40} and Aβ_{42} lost much of their initial α-helicity in favor of random coil and β-strand structures. The resulting structures collapsed over time to form configurations with radii of gyration that agree well with experimental findings[67] and previous simulation results.[68−71] As a result, though each of the simulation sets for monomeric Aβ had only six members, we believe the configurations observed throughout the trajectories to be representative members of a larger conformational ensemble that Aβ samples in vitro and in vivo. Exhaustive sampling of structurally dynamic proteins using atomistic simulations is a difficult task given current computational limitations, though our simulations are extensive, representing 900 ns of accumulated simulation time in each simulation set of Aβ monomers.

Binding of morin to monomeric Aβ_{40} and Aβ_{42} principally affected the tertiary structure of the peptides, diminishing their ability to form hydrophobic contacts and thus impeding the collapse of the structure from its initial α-helical, extended configuration to a more compact, disordered structure. In the context of Aβ_{40}, the binding of morin to the peptide significantly reduced hydrophobic contacts and broadened the minimum of the free energy surface defined by these contacts and the radius of gyration (R_g) of the peptide. Administration of a large molar excess of morin (10:1) augmented these effects, leading to a significant expansion of the peptide structure, as manifested by the increase in R_g relative to the results of the control M40 simulations. The administration of 2:1 morin to the Aβ_{42} peptide had minimal effect on the structure of the peptide, indicating that it is more resilient to this treatment. The 10:1 molar excess of morin to Aβ_{42} caused significant secondary and tertiary structural effects. The free energy minima for Aβ_{42} defined by contacts and R_g showed dual energy minima, indicating two populations of energetically favorable configurations. Thus, we conclude that a greater level of therapeutic compounds would be necessary to inhibit the aggregation of Aβ_{42}, consistent with the results by Ono et al. in their fibril formation assays.[11] Specifically for morin, inhibiting Aβ_{42} fibril formation required nearly three times the concentration of morin than in the case of Aβ_{40} fibril formation. Since fibril formation proceeds through oligomeric intermediates,[72−74] we expect the effects to be similar for these species.

In all of the simulations of Aβ dimerization, we observed that monomers that were initially separated in the simulation cell aggregated to form stable dimers. This behavior was observed regardless of the presence of morin, but important differences can be found in these simulations. It was also observed that the manner in which Aβ_{40} and Aβ_{42} dimerized was different. In the D40 simulations, Aβ_{40} principally associated via both polar and nonpolar (hydrophobic) contacts, forming many close interpeptide interactions between residues in the center of the peptide sequence. Specifically, contacts involving the CHC ($L_{17}VFFA_{21}$) and the flanking peptide sequences were common. In contrast, Aβ_{42} peptides were driven together by hydrophobic contacts involving C-terminal residues, leaving the more polar N-terminal region exposed to solvent. Bitan et al. previously concluded that the manner in which these two alloforms of Aβ aggregated was different, such that the addition of Ile41 and Ala42 to the C-terminus of Aβ (to give the longer and more hydrophobic Aβ_{42} alloform) led to greater stability of low-molecular weight aggregates that more rapidly gave rise to large, insoluble complexes.[75] More recently, Côté et al. also proposed a role for Ile41 and Ala42 in increasing hydrophobic contacts in Aβ_{42} dimers to form a very stable hydrophobic nucleus.[20] In agreement with these previous findings, our simulation results also predict that even at the earliest stages of aggregation (dimer formation), the morphology and stabilizing interpeptide interactions between Aβ_{40} and Aβ_{42} are different.

Dimerization of both Aβ_{40} and Aβ_{42} led to a decrease in total helicity and an increase in β-strand content, relative to the monomeric state. In the M40 simulations, the Aβ_{40} peptides contained, on average, 20 ± 12% β-strand and 7 ± 8% total helix; in the dimeric state (D40 simulations), β-strand content increased slightly to 24 ± 5% and total helicity decreased to 4 ± 4%. With respect to Aβ_{42} dimerization, β-strand content nearly doubled relative to the monomeric state (13 ± 5% in the M42 simulations, 25 ± 13% in the D42 set), while total helicity was reduced from 15 ± 4% to 8 ± 5%. While not in absolute quantitative agreement, the helical and β-strand content observed in the D40 and D42 simulations are in good agreement with the results obtained by Bitan et al. [75] and Côté et al. [20] regarding secondary structure of Aβ in the dimeric state. Further, Kim and Hecht [76] determined that Aβ_{42} has enhanced amyloidogenicity relative to Aβ_{40} due to the added hydrophobicity of residues Ile41 and Ala42 and their propensity to form β-strand structures. In our simulations, D42 dimers were driven together by C-terminal hydrophobic contacts. These residues showed a greater frequency of forming β-strands (in excess of 60% at Ile41, Figure 12D) than the C-terminal residues of Aβ_{40} (approximately 40%, Figure 9D).

Treatment of Aβ_{40} and Aβ_{42} with morin resulted in both interfacial and surface binding of morin. Interfacial binding was classified as the presence of two or more morin molecules at the dimerization interface between the two peptides. Surface binding indicated that morin bound principally on the outer surface of the dimer, such that morin was scattered over the surface. Neither of these binding modes significantly affected the secondary structure content of Aβ_{40} dimers, but the extent of interpeptide interaction was very different in the case of interfacial binding. Specifically, hydrophobic contacts between the two Aβ_{40} peptides were significantly reduced. In contrast, surface binding to Aβ_{40} led to an insignificant decrease in interpeptide contacts and dimer structures that were comparable to controls in terms of their level of compactness. Neither binding mode significantly altered the secondary structure content of the peptides. Binding of morin to Aβ_{42} dimers produced many of the same effects as in the simulations of Aβ_{40}, with several notable differences. While interfacial binding did affect quaternary interactions between the two peptides (heavy atom and hydrophobic contacts), the reduction in contacts was considerable, but not statistically significant, as was the case in the D40$_{\mathrm{M}}$ simulations in which morin bound interfacially. Hydrogen bonding, however, was significantly reduced between the peptides with morin bound in this manner. We hypothesize that the binding of morin may serve to stabilize these dimers in a form that is less conducive to further aggregation and formation of toxic species. That is, while morin was clearly able to weaken interpeptide interactions (particularly when bound interfacially), it may also serve to prevent any conformational rearrangement that would lead to higher-order aggregation, thus locking Aβ in this "off-pathway" state. Further studies would be necessary to confirm this hypothesis. When morin bound to the surface of Aβ_{42} dimers, β-strand content was reduced significantly, with the effect being greatest in the CHC. Binding of morin to polar residues flanking this sequence caused a considerable reduction in β-strand probability, concomitant with an increase in helicity. We propose that this effect arises because morin induces greater rigidity in the Aβ structure and shields it from the polar solvent, an environment that promotes β-strand formation.

Simulations of preformed Aβ dimers (both fibril- and oligomer-derived species) showed that the application of morin had little effect on the structural stability of these structures. Our simulations predict that once formed, Aβ dimers are very resilient when challenged with morin. Simulations of Aβ_{40} and Aβ_{42} dimers produced structures principally composed of β-strand and random coil structures, and their overall size (as measured by R_g) was comparable to experimental results obtained by Walsh et al.[52]

As was the case with the D40$_{\mathrm{M}}$ and D42$_{\mathrm{M}}$ simulations, binding of morin to different regions of the Aβ_{40} and Aβ_{42} peptides had different effects on the preformed dimer structures. Binding to polar residues toward the N-terminus of preformed dimers had little effect on the stability of the peptides, but these interactions did serve to attract morin to Aβ and in many cases acted as a conduit by which morin moved along the peptide sequence toward C-terminal hydrophobic regions and the polar bend region, in which the Asp23-Lys28 salt bridge is present. Interactions between morin and hydrophobic regions of Aβ_{40} and Aβ_{42} showed the greatest level of destabilization in the dimers. We observed considerable twisting and flattening of β-sheets, in addition to backbone destabilization in the areas with which morin interacted, in all of the simulations of preformed dimers in the presence of morin (P40$_{\mathrm{M}}$, L42$_{\mathrm{M}}$, and Y42$_{\mathrm{M}}$).

Our previous work[12] with the pentameric form of the L42 model (a so-called "protofibril") in the presence and absence of morin indicated that morin interacted with the Asp23-Lys28 salt bridges in the pentamer, using this region to penetrate into the hydrophobic core of the protofibril and disrupt backbone interactions. While we see some binding of morin to this same region of the Aβ_{42} peptide in the L42$_{\mathrm{M}}$ simulations, the destabilizing effect is not observed to the same extent. This apparent discrepancy can be largely attributed to the reduced stability of the Asp23-Lys28 salt bridges in the L42 dimers. Interpeptide salt bridges that were very stable in the protofibril were unstable in the dimeric form of the L42 structure due to the greater solvent exposure of these groups. Without a rigid binding site, morin interacted more weakly with the L42 dimer than with the protofibril form of L42, causing only transient destabilization of backbone hydrogen bonding in the L42$_{\mathrm{M}}$ simulations. It has been proposed that Asp23-Lys28 salt bridges are less stable in oligomeric forms of Aβ than in the mature protofibril or fibril forms,[17] in which case the morin-susceptible region in the L42 structure may be absent in these structures, resulting in a weaker affinity between morin and Aβ_{42} and binding occurring in multiple locations. The addition of morin to the dimeric structures led to twisting and flattening of the β-sheet structures that was largely absent in the protofibril structures. Instead, in the larger, more rigid pentameric protofibrils, a monomer of Aβ partially dissociated from the core of the pentamer. The size and inherent rigidity of the protofibril led to the disruption of the Asp23-Lys28 salt bridge and backbone hydrogen bonding.

Recent work by Ladiwala et al.[77] concluded that the polyphenol myricetin, which is structurally very similar to morin, did not prevent the aggregation of Aβ, but instead was capable of remodeling prefibrillar oligomers and fibrils into unstructured, insoluble aggregates. They concluded that condensation of Aβ monomers was indeed possible, even in the presence of such molecules, and our results agree with those findings. Though we found that both Aβ_{40} and Aβ_{42} formed dimers from initially separated monomers, we have described many differences between the control (untreated) structures and those that formed in the presence of morin. Ladiwala et al. concluded that myricetin and related compounds promoted nonspecific interactions between Aβ monomers, a theory that is directly supported by the results obtained in the present work. Further, Ladiwala et al. predicted that myricetin could remodel existing soluble oligomers into disordered aggregates that would not lead to fibril formation. The structural deformations (overall structural twisting and flattening of β-strands) seen in our preformed dimer simulations in the presence of morin, though subtle, represent possible outcomes that would divert oligomeric species from becoming fibrils or other higher-order aggregated structures.

The results we present here are also compatible with recent work by Convertino et al.,[78] who used MD simulations to determine that the intrinsic disorder of the Aβ^{12-28} fragment precluded any shared binding mode among diverse compounds containing aromatic groups. Local effects on the structure of the peptide sequence were largely dependent upon specific interactions that arose between Aβ and the library of test compounds. The secondary structure propensities we have determined in the present work for full-length Aβ_{40} and Aβ_{42} (Figures 9 and 12) agree well with their findings with respect to the structure of the peptide fragment in their study. Notably, we found that binding of morin near residues of the CHC caused a marked decrease in the appearance of β-strand structures in the D42$_{\mathrm{M}}$ simulations (Figure 12); thus morin induced its effect via long-range interactions. Morin did not bind directly to the CHC sequence, but rather to residues flanking it. These results agree well with the prediction by Convertino et al. that Aβ aggregation inhibitors may act at indirect or allosteric sites to influence peptide structure.

■ CONCLUSION

In the present work, we have used extensive explicit-solvent, atomistic MD simulations to describe the interactions of the flavonoid morin with monomeric and dimeric Aβ_{40} and Aβ_{42} in an attempt to understand the means by which this compound inhibits Aβ aggregation. We found that binding of morin to monomeric Aβ alters the free energy surface defined by tertiary interactions within the peptide, altering its ability to collapse and form a stable hydrophobic nucleus. Dimerization was not prevented by the administration of morin, but the structure of newly formed Aβ dimers was affected by the binding location of morin, either at the dimerization interface or the surface of the aggregate. While we cannot rule out that the binding locations of morin were limited by incomplete sampling, we believe the present work to be the most extensive to date in the investigation of morin binding to Aβ monomers and dimers, and thus represents a plausible model for in vitro and in vivo behavior. Additional studies utilizing enhanced sampling techniques may be useful in further understanding the implications of these binding poses.

Interpeptide contacts and secondary structural elements were differentially affected by the binding location of morin, with tertiary and quaternary interactions most consistently modulated by the presence of morin. In the context of preformed Aβ dimers, application of morin had only minimal effects, which were again dependent on the location along the peptide sequence to which morin binds. The regions on the peptide that gave rise to the largest structural changes (in this case, tertiary and quaternary interactions) are the CHC and polar bend region. We thus conclude that, along with minor changes in secondary structure propensities, the main effect that morin has on the structure of Aβ_{40} and Aβ_{42} in the monomeric and dimeric states is to alter tertiary and quaternary interactions that give rise to structures that are measurably different from controls. These results provide molecular insight into the nature of so-called "off-pathway" aggregates that may have reduced toxicity compared to untreated, soluble Aβ aggregates, the principal toxic entity in Alzheimer's disease.

■ ASSOCIATED CONTENT

Ⓢ Supporting Information

Thirteen figures, presenting the initial configurations of morin-containing Aβ monomer systems, morin−Aβ contact residency time, and morin−Aβ contacts per residue, are provided. This material is available free of charge via the Internet at http://pubs.acs.org.

■ AUTHOR INFORMATION

Corresponding Author

*E-mail: drbevan@vt.edu. Address: 111 Engel Hall Blacksburg, VA 24061. Phone: (540) 231-5040. Fax: (540) 231-9070.

Funding

The material is based upon work supported by the Macromolecular Interfaces with Life Sciences (MILES) Integrative Graduate Education and Research Traineeship (IGERT) of the National Science Foundation under Agreement DGE-0333378, and by the Institute for Critical Technology and Applied Science (ICTAS) at Virginia Tech.

Notes

The authors declare no competing financial interest.

■ ACKNOWLEDGMENTS

The authors thank Dr. Robert Tycko for providing the coordinates of Aβ_{40} fibrils, Dr. Liping Yu for providing the coordinates of the soluble Aβ_{42} dimer, and Advanced Research Computing at Virginia Tech for computing time on the SystemX and Athena supercomputers.

■ REFERENCES

(1) Hardy, J. A., and Higgins, G. A. (1992) Alzheimer's disease: The amyloid cascade hypothesis. *Science 256*, 184−185.

(2) Kayed, R., Head, E., Thompson, J. L., McIntire, T. M., Milton, S. C., Cotman, C. W., and Glabe, C. G. (2003) Common structure of soluble amyloid oligomers implies common mechanism of pathogenesis. *Science 300*, 486−489.

(3) Kayed, R., Sokolov, Y., Edmonds, B., McIntire, T. M., Milton, S. C., Hall, J. E., and Glabe, C. G. (2004) Permeabilization of lipid bilayers is a common conformation-dependent activity of soluble amyloid oligomers in protein misfolding diseases. *J. Biol. Chem. 279*, 46363−46366.

(4) Thinakaran, G., and Koo, E. H. (2008) Amyloid precursor protein trafficking, processing, and function. *J. Biol. Chem. 283*, 29615−29619.

(5) Haass, C., and Selkoe, D. J. (2007) Soluble protein oligomers in neurodegeneration: lessons from the Alzheimer's amyloid β-peptide. *Nat. Rev. Mol. Cell Biol. 8*, 101−112.

(6) Barten, D. M., and Albright, C. F. (2008) Therapeutic strategies for Alzheimer's disease. *Mol. Neurobiol. 37*, 171−186.

(7) Saura, C. A., Choi, S.-Y., Beglopoulos, V., Malkani, S., Zhang, D., Rao, B. S. S., Chattarji, S., Kelleher, R. J., III, Kandel, E. R., Duff, K., Kirkwood, A., and Shen, J. (2004) Loss of presenilin function causes impairments of memory and synaptic plasticity followed by age-dependent neurodegeneration. *Neuron 42*, 23−36.

(8) Gestewicki, J. E., Crabtree, G. R., and Graef, I. A. (2004) Harnessing chaperones to generate small-molecule inhibitors of amyloid β aggregation. *Science 306*, 865−869.

(9) Ono, K., Hamaguchi, T., Naiki, H., and Yamada, M. (2006) Anti-amyloidogenic effects of antioxidants: implications for the prevention and therapeutics of Alzheimer's disease. *Biochim. Biophys. Acta 1762*, 575−586.

(10) Havsteen, B. H. (2002) The biochemistry and medical significance of the flavonoids. *Pharmacol. Ther. 96*, 67−202.

(11) Ono, K., Yoshiike, Y., Takashima, A., Hasegawa, K., Naiki, H., and Yamada, M. (2003) Potent anti-amyloidogenic and fibril-destabilizing effects of polyphenols *in vitro*: implications for the prevention and therapeutics of Alzheimer's disease. *J. Neurochem. 87*, 172−181.

(12) Lemkul, J. A., and Bevan, D. R. (2010) Destabilizing Alzheimer's Aβ_{42} protofibrils with morin: Mechanistic insights from molecular dynamics simulations. *Biochemistry 49*, 3935−3946.

(13) Flöck, D., Colacino, S., Colombo, G., and Di Nola, A. (2006) Misfolding of the amyloid β-protein: A molecular dynamics study. *Proteins: Struct. Funct. Bioinform. 62*, 183−192.

(14) Luttmann, E., and Fels, G. (2006) All-atom molecular dynamics studies of the full-length β-amyloid peptides. *Chem. Phys. 323*, 138−147.

(15) Liu, F.-F., Ji, L., Dong, X.-Y., and Sun, Y. (2009) Molecular insight into the inhibition effect of trehalose on the nucleation and elongation of amyloid β-peptide oligomers. *J. Phys. Chem. B 113*, 11320−11329.

(16) Lee, C., and Ham, S. (2011) Characterizing amyloid-beta protein misfolding from molecular dynamics simulations with explicit water. *J. Comput. Chem. 32*, 349−355.

(17) Tarus, B., Straub, J. E., and Thirumalai, D. (2006) Dynamics of Asp23-Lys28 salt-bridge formation in Aβ_{10-35} monomers. *J. Am. Chem. Soc. 128*, 16159−16168.

(18) Tarus, B., Straub, J. E., and Thirumalai, D. (2008) Structures and free-energy landscapes of the wild type and mutants of the Aβ_{21-30} peptide are determined by an interplay between intrapeptide electrostatic and hydrophobic interactions. *J. Mol. Biol. 379*, 815−829.

(19) Urbanc, B., Betnel, M., Cruz, L., Bitan, G., and Teplow, D. B. (2010) Elucidation of amyloid β-protein oligomerization mechanisms: discrete molecular dynamics study. *J. Am. Chem. Soc. 132*, 4266−4280.

(20) Côté, S., Laghaei, R., Derreumaux, P., and Mousseau, N. (2012) Distinct dimerization for various alloforms of the amyloid-beta protein: Aβ_{1-40}, Aβ_{1-42}, and Aβ_{1-40}(D23N). *J. Phys. Chem. B 116*, 4043−4055.

(21) Mitternacht, S., Staneva, I., Härd, T., and Irbäck, A. (2010) Comparing the folding free-energy landscapes of Aβ42 variants with different aggregation properties. *Proteins: Struct. Funct. Bioinform 78*, 2600−2608.

(22) Mitternacht, S., Staneva, I., Härd, T., and Irbäck, A. (2011) Monte Carlo study of the formation and conformational properties of dimers of Aβ42 variants. *J. Mol. Biol. 410*, 357−367.

(23) Coles, M., Bicknell, W., Watson, A. A., Fairlie, D. P., and Craik, D. J. (1998) Solution structure of amyloid β-peptide(1−40) in a water-micelle environment. Is the membrane-spanning domain where we think it is? *Biochemistry 37*, 11064−11077.

(24) Crescenzi, O., Tomaselli, S., Guerrini, R., Salvadori, S., D'Ursi, A. M., Temussi, P. A., and Picone, D. (2002) Solution structure of the Alzheimer amyloid β-peptide (1−42) in an apolar microenvironment: Similarity with a virus fusion domain. *Eur. J. Biochem. 269*, 5642−5648.

(25) Petkova, A. T., Yau, W.-M., and Tycko, R. (2006) Experimental constraints on quaternary structure in Alzheimer's β-amyloid fibrils. *Biochemistry 45*, 498−512.

(26) Lührs, T., Ritter, C., Adrian, M., Riek-Loher, D., Bohrmann, B., Döbeli, H., Schubert, D., and Riek, R. (2005) 3D structure of Alzheimer's amyloid-β(1−42) fibrils. *Proc. Natl. Acad. Sci. U.S.A. 102*, 17342−17347.

(27) Yu, L., Edalji, R., Harlan, J. E., Holzman, T. F., Lopez, A. P., Labkovsky, B., Hillen, H., Barghorn, S., Ebert, U., Richardson, P. L., Miesbauer, L., Solomon, L., Bartley, D., Walter, K., Johnson, R. W., Hajduk, P. J., and Olejniczak, E. T. (2009) Structural characterization of a soluble amyloid β-peptide oligomer. *Biochemistry 48*, 1870−1877.

(28) Zhang, W., Hou, T., Schafmeister, C., Ross, W. S., Case, D. A. LEaP and gleap.

(29) Masman, M. F., Eisel, U. L. M., Csizmadia, I. G., Penke, B., Enriz, R. D., Marrink, S. J., and Luiten, P. G. M. (2009) *In Silico* Study of Full-Length Amyloid β 1−42 Tri- and Penta-Oligomers in Solution. *J. Phys. Chem. B 113*, 11710−11719.

(30) Humphrey, W., Dalke, A., and Schulten, K. (1996) VMD: Visual Molecular Dynamics. *J. Mol. Graphics 14*, 33−38.

(31) Oostenbrink, C., Villa, A., Mark, A. E., and van Gunsteren, W. F. (2004) A biomolecular force field based on the free enthalpy of hydration and solvation: the GROMOS force-field parameter sets 53A5 and 53A6. *J. Comput. Chem. 25*, 1656−1676.

(32) Berendsen, H. J. C., Postma, J. P. M., van Gunsteren, W. F., Hermans, J. (1981) Interaction models for water in relation to protein hydration, In *Intermolecular Forces* (Pullman, B., Ed.) p 331, Reidel, Dordrecht.

(33) Liu, F.-F., Dong, X.-Y., He, L., Middelberg, A. P. J., and Sun, Y. (2011) Molecular insight into conformational transition of amyloid β-peptide 42 inhibited by (−)-epigallocatechin-3-gallate probed by molecular simulations. *J. Phys. Chem. B 115*, 11879−11887.

(34) Takeda, T., Chang, W. E., Raman, E. P., and Klimov, D. K. (2010) Binding of non-steroidal anti-inflammatory drugs to Aβ fibril. *Proteins: Struct. Funct. Bioinform. 78*, 2849−2860.

(35) Raman, E. P., Takeda, T., and Klimov, D. K. (2009) Molecular dynamics simulations of ibuprofen binding to Aβ peptides. *Biophys. J. 97*, 2070−2079.

(36) Hess, B., Kutzner, C., van der Spoel, D., and Lindahl, E. (2008) GROMACS 4: Algorithms for highly efficient, load-balanced, and scalable molecular simulation. *J. Chem. Theory Comput. 4*, 435−447.

(37) Berendsen, H. J. C., Postma, J. P. M., van Gunsteren, W. F., DiNola, A., and Haak, J. R. (1984) Molecular dynamics with coupling to an external bath. *J. Chem. Phys. 81*, 3684−3690.

(38) Nosé, S. (1984) A unified formulation of the constant temperature molecular dynamics methods. *J. Chem. Phys. 81*, 511−519.

(39) Hoover, W. G. (1985) Canonical dynamics: Equilibrium phase-space distributions. *Phys. Rev. A: At. Mol. Opt. Phys. 31*, 1695−1697.

(40) Parrinello, M., and Rahman, A. (1981) Polymorphic transitions in single crystals: A new molecular dynamics method. *J. Appl. Phys. 52*, 7182−7190.

(41) Nosé, S., and Klein, M. L. (1983) Constant pressure molecular dynamics for molecular systems. *Mol. Phys. 50*, 1055−1076.

(42) Hess, B. (2008) P-LINCS: A parallel linear constraint solver for molecular simulation. *J. Chem. Theory Comput. 4*, 116−122.

(43) Darden, T., York, D., and Pedersen, L. (1993) Particle mesh Ewald: an N·log(N) method for Ewald sums in large systems. *J. Chem. Phys. 98*, 10089−10092.

(44) Essmann, U., Perera, L., Berkowitz, M. L., Darden, T., Lee, H., and Pedersen, L. G. (1995) A smooth particle mesh Ewald method. *J. Chem. Phys. 103*, 8577−8593.

(45) Kabsch, W., and Sander, C. (1983) Dictionary of protein secondary structure: Pattern recognition of hydrogen-bonded and geometrical features. *Biopolymers 22*, 2577−2637.

(46) Tjernberg, L. O., Näslund, J., Lindqvist, F., Johansson, J., Karlström, A. R., Terenius, L., and Nordstedt, C. (1996) Arrest of β-amyloid fibril formation by a pentapeptide ligand. *J. Biol. Chem. 271*, 8545−8548.

(47) Jarrett, J. T., and Lansbury, P. T., Jr. (1993) Seeding of "one-dimensional crystallization" of amyloid: a pathogenic mechanism in Alzheimer's disease and scrapie? *Cell 73*, 1055−1058.

(48) Harper, J. D., and Lansbury, P. T., Jr. (1997) Models of amyloid seeding in Alzheimer's disease and scrapie: mechanistic truths and physiological consequences of the time-dependent solubility of amyloid proteins. *Annu. Rev. Biochem. 66*, 385−407.

(49) Ma, B., and Nussinov, R. (2006) Simulations as analytical tools to understand protein aggregation and predict amyloid conformation. *Curr. Opin. Chem. Biol. 10*, 445−452.

(50) Buchete, N.-V., Tycko, R., and Hummer, G. (2006) Molecular dynamics simulations of Alzheimer's β-amyloid protofibrils. *J. Mol. Biol. 353*, 804−821.

(51) Fawzi, N. L., Kohlstedt, K. L., Okabe, Y., and Head-Gordon, T. (2008) Protofibril assemblies of the Arctic, Dutch, and Flemish mutants of the Alzheimer's Aβ_{1-40} peptide. *Biophys. J. 94*, 2007−2016.

(52) Walsh, D. M., Lomakin, A., Benedek, G. B., Condron, M. M., and Teplow, D. B. (1997) Amyloid β-protein fibrillogenesis. *J. Biol. Chem. 272*, 22364−22732.

(53) Matthes, D., and de Groot, B. L. (2009) Secondary structure propensities in peptide folding simulations: a systematic comparison of molecular mechanics interaction schemes. *Biophys. J. 97*, 599−608.

(54) Best, R. B., Buchete, N.-V., and Hummer, G. (2008) Are current molecular dynamics force fields too helical? *Biophys. J. 95*, L07−L09.

(55) van Gunsteren, W. F., Berendsen, H. J. C. (1987) *Groningen Molecular Simulation (GROMOS) Library Manual*, BIOMOS b.v., Groningen.

(56) van Gunsteren, W. F., Billeter, S., Eising, A., Hünenberger, P., Krueger, P., Mark, A. E., Scott, W., Tironi, I. (1996) *Biomolecular Simulations: the GROMOS96 Manual and User Guide*, BIOMOS b.v., Groningen.

(57) Kaminski, G. A., Friesner, R. A., Tirado-Rives, J., and Jorgensen, W. L. (2001) Evaluation and reparametrization of the OPLS-AA force field for proteins via comparison with accurate quantum chemical calculations on peptides. *J. Phys. Chem. B 105*, 6474−6487.

(58) Wang, J., Cieplak, P., and Kollman, P. A. (2000) How well does a restrained electrostatic potential (RESP) model perform in calculating conformational energies of organic and biological molecules? *J. Comput. Chem. 21*, 1049−1074.

(59) Hornak, V., Abel, R., Okur, A., Strockbine, B., Roitberg, A., and Simmerling, C. (2006) Comparison of multiple Amber force fields and development of improved protein backbone parameters. *Proteins: Struct. Funct. Bioinform. 65*, 712−725.

(60) Sgourakis, N. G., Yan, Y., McCallum, S. A., Wang, C., and Garcia, A. E. (2007) The Alzheimer's peptides Aβ40 and 42 adopt distinct conformations in water: a combined MD/NMR study. *J. Mol. Biol. 368*, 1448−1457.

(61) Sgourakis, N. G., Merced-Serrano, M., Boutsidis, C., Drineas, P., Du, Z., Wang, C., and Garcia, A. E. (2011) Atomic-level characterization of the ensemble of the Aβ(1−42) monomer in water using unbiased molecular dynamics simulations and spectral algorithms. *J. Mol. Biol. 405*, 570−583.

(62) Velez-Vega, C., and Escobedo, F. A. (2011) Characterizing the structural behavior of selected Aβ-42 monomers with different solubilities. *J. Phys. Chem. B 115*, 4900−4910.

(63) Chong, S.-H., Park, M., and Ham, S. (2012) Structural and thermodynamic characteristics that seed aggregation of amyloid-β protein in water. *J. Chem. Theory Comput. 8*, 724−734.

(64) Maupetit, J., Tuffery, P., and Derreumaux, P. (2007) A coarse-grained protein force field for folding and structure prediction. *Proteins: Struct. Funct. Bioinform. 69*, 394−408.

(65) Côté, S., Derreumaux, P., and Mousseau, N. (2011) Distinct morphologies for amyloid beta protein monomer: $A\beta_{1-40}$, $A\beta_{1-42}$, and $A\beta_{1-40}$(D23N). *J. Chem. Theory Comput. 7*, 2584−2592.

(66) Olubiyi, O. O., and Strodel, B. (2012) Structures of the amyloid β-peptides $A\beta_{1-40}$ and $A\beta_{1-42}$ as influenced by pH and a D-peptide. *J. Phys. Chem. B 116*, 3280−3291.

(67) Nag, S., Sarkar, B., Bandyopadhyay, A., Sahoo, B., Sreenivasan, V. K. A., Kombrabail, M., Muralidharan, C., and Maiti, S. (2011) Nature of the amyloid-β monomer and the monomer-oligomer equilibrium. *J. Biol. Chem. 286*, 13827−13833.

(68) Massi, F., Peng, J. W., Lee, J. P., and Straub, J. E. (2001) Simulation study of the structure and dynamics of the Alzheimer's amyloid peptide congener in solution. *Biophys. J. 80*, 31−44.

(69) Baumketner, A., Bernstein, S. L., Wyttenbach, T., Lazo, N. D., Teplow, D. B., Bowers, M. T., and Shea, J.-E. (2006) Structure of the 21−30 fragment of amyloid β-protein. *Protein Sci. 15*, 1239−1247.

(70) Raffa, D. F., and Rauk, A. (2007) Molecular dynamics study of the beta amyloid peptide of Alzheimer's disease and its divalent copper complexes. *J. Phys. Chem. B 111*, 3789−3799.

(71) Baumketner, A., and Shea, J.-E. (2006) Folding landscapes of the Alzheimer amyloid-β(12−28) peptide. *J. Mol. Biol. 362*, 567−579.

(72) Lomakin, A., Chung, D. S., Benedek, G. B., Kirschner, D. A., and Teplow, D. B. (1996) On the nucleation and growth of amyloid β-protein fibrils: Detection of nuclei and quantitation of rate constants. *Proc. Natl. Acad. Sci. U.S.A. 93*, 1125−1129.

(73) Pellarin, R., and Caflisch, A. (2006) Interpreting the aggregation kinetics of amyloid peptides. *J. Mol. Biol. 360*, 882−892.

(74) Fawzi, N. L., Okabe, Y., Yap, E.-H., and Head-Gordon, T. (2007) Determining the critical nucleus and mechanism of fibril elongation of the Alzheimer's $A\beta_{1-40}$ peptide. *J. Mol. Biol. 365*, 535−550.

(75) Bitan, G., Kirkitadze, M. D., Lomakin, A., Vollers, S. S., Benedek, G. B., and Teplow, D. B. (2003) Amyloid β-protein (Aβ) assembly: Aβ40 and Aβ42 oligomerize through distinct pathways. *Proc. Natl. Acad. Sci. U.S.A. 100*, 330−335.

(76) Kim, W., and Hecht, M. H. (2005) Sequence determinants of enhanced amyloidogenicity of Alzheimer Aβ42 peptide relative to Aβ40. *J. Biol. Chem. 280*, 35069−35076.

(77) Ladiwala, A. R. A., Dordick, J. S., and Tessier, P. M. (2011) Aromatic small molecules remodel toxic soluble oligomers of amyloid β through three independent pathways. *J. Biol. Chem. 286*, 3209−3218.

(78) Convertino, M., Vitalis, A., and Caflisch, A. (2011) Disordered binding of small molecules to Aβ(12−28). *J. Biol. Chem. 286*, 41578−41588.